The Use of a Synthetic Binary Solid Solution to Model Igneous Textural Evolution

A thesis presented to the Faculty

Of the University at Albany, State University of New York

In partial fulfillment of the requirements

For the degree of

Master of Science

College of Arts & Sciences

Department of Earth and Atmospheric Sciences

Elizabeth Scott
2002

The Use of a Synthetic Binary Solid Solution to Model Igneous Textural Evolution

Abstract of

A thesis presented to the Faculty

Of the University at Albany, State University of New York

In partial fulfillment of the requirements

For the degree of

Master of Science

College of Arts & Sciences

Department of Earth and Atmospheric Sciences

Elizabeth Scott
2002

Abstract

Crystallization experiments using a synthetic igneous analog have shown that grain boundary migration can take place in melt-present environments (Means and Park, 1994). In order to evaluate the importance of metamorphic processes during the textural evolution of a crystal mush, microstructural evidence is needed to link them with final igneous textures. In natural magmatic systems, plagioclase may provide a microstructural link; plagioclase solid solution enables the process of chemical zoning and preserves a record of crystal morphology (and chemistry) during growth. If metamorphic processes are common, they should affect the zoning patterns of plagioclase crystals.

A petrographic stage heater apparatus was designed and built for the purpose of observing crystallization processes with a new plagioclase analog. The analog utilized synthetic compounds within the (K, NH_4)SCN system and was crystallized at low temperatures (< 172 °C) for observation *in situ* with an optical microscope. The melting points of compounds containing X_K = (0, 0.25, 0.50, 0.75, 1) were measured in both thin section and in sealed capillary tubes in order to construct a phase diagram. Compounds of intermediate composition X_K = (0.25, 0.50, 0.75) created a continuous solid solution with initial and final melting points between 82 °C and 171 – 175 °C in thin section, and between 108 °C and 144 °C (± 1) in sealed capillary tubes. The differences between the two data sets are probably due to the absorption of atmospheric water and differing abilities of the two systems to contain the water.

Textural studies of quenched compounds with composition X_K = 0.8 and X_K = 0.75 resulted in the formation of crystals with concentric extinction patterns (under cross polarized light) that resemble patterns produced by chemical zoning in plagioclase. Grain boundary migration was also observed between chemically homogenous grains within the solid solution. However, relatively slow rates of cooling were required to produce grain boundary migration. While grain boundary migration was only observed in unzoned solid solution crystals, further crystallization experiments utilizing faster rates of cooling may produce grain boundary migration in chemically zoned crystals.

Acknowledgements

Without Win Means, this project would not have begun.

Without John Arnason, creativity and madness would have been one.

Without my family, my vision would have been lost.

I would like to thank John, Win, Ian, and Emerson.

Table of Contents

Chapter 1: Introduction p. 1 - 10

- 1.1 Purpose
- 1.2 Background: (1) High temperature laboratory crystallization of feldspars
- 1.3 Background: (2) Synthetic crystallization experiments

Chapter 2: Mineralogy and Crystal Chemistry; Plagioclase Solid Solution and Potassium – Ammonium Thiocyanate Solid Solution p.11 - 33

- 2.1 Plagioclase: Albite ($NaAlSi_3O_8$) – Anorthite ($CaAl_2SiO_8$)
  - 2.1a Morphology
  - 2.1b Crystallography
  - 2.1c Crystal chemistry
  - 2.1d Optics
  - 2.1e Chemical zoning
  - 2.1f Liquidus phase relations
  - 2.1g Sub-solidus phase relations
- 2.2 (K, NH_4)SCN Solid Solution
  - 2.1a Morphology
  - 2.1b Crystallography
  - 2.1c Crystal chemistry
  - 2.1d Optics
  - 2.1e Phase relations
- 2.3 Comparison between plagioclase and its (K, NH_4)SCN analogue

Chapter 3: Experimental design p. 34 - 47

- 3.1 Apparatus
- 3.2 Designing a synthetic igneous analog capable of solid solution
- 3.3 Crystallization experiments
  - 3.3a Thin section preparation of a two-component system: KSCN – NH_4SCN
  - 3.3b Thin section preparation of a four-component system: KSCN – NH_4SCN NH_4Cl – $(NH_4)_2[Co(SCN)_4] \cdot nH_2O$
  - 3.3c Sample preparation: sealed capillary tube experiments
- 3.4 Error

Chapter 4: Phase Relation Experiments with the (K, NH_4)SCN Solid Solution p. 48 - 52

- 4.1 Phase relations produced from thin section experiments
- 4.2 Phase relations obtained from capillary tube experiments

Chapter 5: Textural Experiments with the (K, NH_4)SCN Solid Solution p. 53 - 58

- 5.1 Two component system: KSCN – NH_4SCN
- 5.2 Four component system: KSCN – NH_4SCN – NH_4Cl – $(NH_4)_2[Co(SCN)_4] \cdot nH_20$
- 5.3 Results
- 5.4 Discussion

Chapter 6: Conclusion p. 59 – 60

References p. 61 - 64

Appendices p. 65 – 83

- A.1 Table III: Capillary tube experimental data
- A.2 Table IV: Thin section experimental data
- A.3 Photomicrograph Series I – Series VIII (including experimental details)
- A.4 Stage heater apparatus engineering diagram

List of Figures

Figure 1. Illustration of a grain boundary common to large intrusions, and microstructural interpretation. p. 2

Figure 2. Photomicrographs of plagioclase crystals from the Stillwater Complex of Montana. p. 4

Figure 3. Three-component system created by Means and Park (1994). p. 10

Figure 4. Albite morphology and twinning. p. 13

Figure 5. Principle feldspar lattice structures. p. 13

Figure 6. The crank-shaft structure and tetrahedral rings specific to feldspar. p. 15

Figure 7. The Al – Si ordering pattern in celsian and anorthite. p. 15

Figure 8. Concentric zoning of an anhedral crystal that indicates prior euhedral growth. p. 18

Figure 9. Equilibrium phase diagram for the system albite – anorthite at constant pressure. p. 20

Figure 10. Photomicrograph of NH_4SCN and melt in plane polarized light. p. 23

Figure 11. Plots demonstrating the effects of temperature and composition on unit cell parameters for the $(K, NH_4)SCN$ solid solution. p. 25

Figure 12. Representation of the NH_4SCN crystal structure. p. 26

Figure 13. Photomicrographs of solid solution crystals with composition $X_K = 1$, $X_K = 0$, and $X_K = 0.8$. p. 28, 29

Figure 14. Phase diagram of the KSCN – NH_4SCN solid solution constructed from published and commercial sources. p. 30

Figure 15. The ordering of the SCN ion due to temperature change. p. 32

Figure 16. Diagram of the stage heater apparatus. p. 35

Figure 17. Cut-away view of the stage heater. p. 35

Figure 18. Components of thin-sections used for determining $(K, NH_4)SCN$ phase relations. p. 41

Figure 19. Diagram of a capillary tube sample. p. 44

Figure 20. T – X phase diagram of the (K, NH_4)SCN solid solution obtained from observations in thin-section. p. 49

Figure 21. T – X phase diagram of the (K, NH_4)SCN solid solution obtained from capillary tube data. p. 51

Figure 22. Photomicrographs of solid solution crystals of composition X_K = 0.75 that exhibit apparent zoning patterns. p. 55

Figure 23. Series of photomicrographs showing the growth of "white phase" solid solution crystals in the presence of melt; grain boundary migration is evident. p. 58

Figure 24. Series of photomicrographs showing the growth of "white phase" solid solution crystals in the presence of melt. p. 58

List of Tables

Table I. Plagioclase symmetry elements and unit cell parameters. p. 7

Table II. (K, NH_4)SCN symmetry elements and unit cell parameters. p. 17

Appendix

Table III. Phase relation data acquired from thin section samples. p. 68

Table IV. Phase relation data acquired from capillary tube samples p. 70

Chapter 1

Introduction

The textural relationships of minerals in plutonic rocks are commonly thought to give a great deal of information about magmatic processes. They are used to interpret crystallization sequences (e.g. Wager and Brown, 1960; Jackson, 1961; Hunter, 1987) and to track the evolution of porosity and permeability within a crystal mush, (e.g. Hunter, 1996). Interpretations of igneous textures also influence our understanding of many important factors including: mass and energy transfer within a melt, melt extraction (Hunter, 1996), and processes affecting the distribution of trace elements (e.g. Mittlefehldt and Miller, 1983).

Igneous petrographers commonly use crystal habit and impingement relationships to determine the crystallization paths of plutonic rocks. Most textural interpretations, such as order of crystallization, are obtained by applying logical principles to grain boundary relationships observed in thin-section. For example, when a grain boundary is shared by two crystals that significantly differ in crystal face development, (i.e. a euhedral crystal and an anhedral crystal) the euhedral crystal is commonly interpreted as having formed first.

Figure 1 illustrates an ideal situation in which two crystals share a grain boundary. Crystal A is euhedral and appears to have grown unhindered. The boundary of crystal B is interrupted by crystal A, making it appear as if crystal A interfered with its growth. If this process interpretation is correct, then crystal A was present in the crystal mush before crystal B.

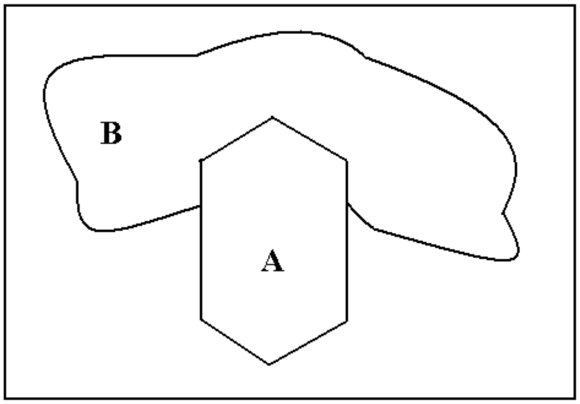

Figure 1. In a plutonic rock, the grain boundary between crystals A and B would suggest that crystal A formed first and crystal B formed second. (Note; in a metamorphic rock, crystal B might be interpreted as having formed first, and crystal A second.)

Many large mafic intrusions contain rocks with poikilitic texture (similar to the cartoon texture shown in Figure 1) in which euhedral crystals are contained within larger anhedral host crystals. Figure 2 includes photomicrographs of plagioclase crystals from the Stillwater Complex of Montana. Figure 2(A) was taken in plane polarized light, and Figure 2(B) was taken in cross polarized light. Both photomicrographs show that plagioclase crystals have developed 120° dihedral angles that may have been achieved through grain boundary migration. Figure 2(B), taken under cross polarized light, reveals that the largest crystal in the field of view (centrally located) is also concentrically zoned. Without the ability to observe paths of crystallization, however, unassailable conclusions cannot be drawn about the textural evolution of crystal mushes.

Microstructural interpretation forms the basis of modern cumulus theory and has been used to interpret Skaergaard, Stillwater, and Bushveld magmatic evolution (Barnes and Maier, 2002; Hunter, 1987; Jackson, 1954; Jackson, 1961; McBirney, 1995; Tacinelli and Naslund, 1990; Thayer and Jackson, 1972; Wager and Brown, 1960). Textural interpretations, however, are based upon the appearance of grain boundary geometries within plutonic rocks. These boundaries may or may not resemble the grain boundary relationships present during crystallization. Without the ability to observe crystallization processes *in situ*, interpretations based upon final textures cannot be fully proven.

While the high temperatures and pressures of large intrusions prohibit the direct observation of natural, silicate crystallization processes, work by Means and Park (1994) demonstrated that low-temperature synthetic crystallization experiments provide a "window" to the types of processes that may be taking place during plutonic textural evolution. The synthetic igneous analogue developed by Means and Park (1994) is a

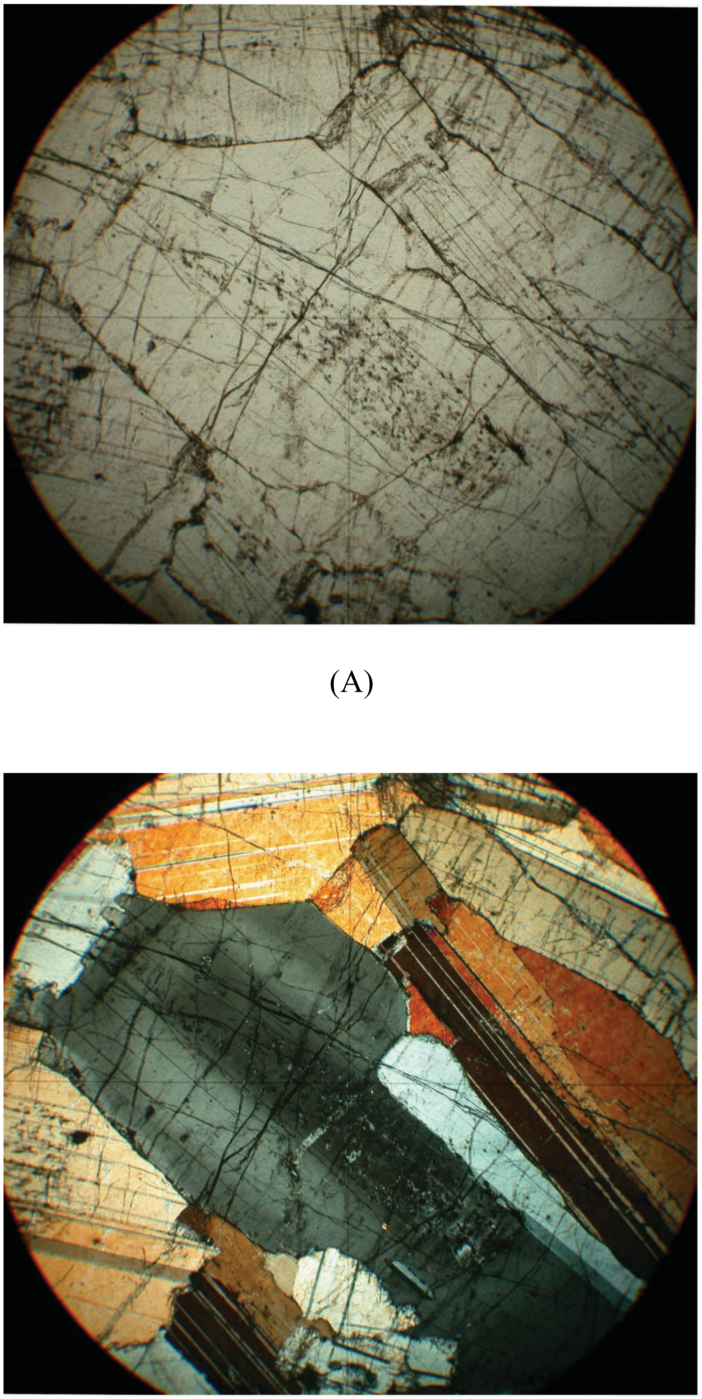

(A)

(B)

Figure 2. Photomicrographs of plagioclase crystals from the Stillwater Complex of Montana. Photomicrograph (A) was taken in plane polarized light and photomicrograph (B) was taken of the same crystals in cross polarized light. Both photomicrographs show grain boundaries with 120° dihedral angles, indicating some degree of grain boundary adjustment. Cross polarized light in photomicrograph B also reveals that the largest plagioclase crystal (in the middle of the field of view) is concentrically zoned.

three-component, eutectic system in which crystallization occurs below 100 °C and is observable *in situ* with a microscope. Means and Park (1994) observed grain and phase boundary migration in the presence of synthetic melt, and if these processes are common in igneous systems, then interpretations of magmatic evolution based upon textural relationships may need revision.

1.1 Purpose

In order to evaluate the importance of grain boundary migration during the textural evolution of a crystal mush, a microstructural link is needed between the process of grain boundary migration and final igneous textures. In natural magmatic systems, plagioclase may provide a microstructural link; plagioclase solid solution enables the process of chemical zoning and preserves a record of crystal morphology (and chemistry) during growth. If the occurrence of grain boundary migration is common, its “signature” should be reflected in the zoning patterns of plagioclase crystals.

Grain boundary migration induced during the growth of synthetic, chemically zoned crystals might produce a grain boundary migration “signature” that could then be compared to plagioclase zoning patterns in igneous rocks. Thus, information about whether or not the process is significant during magmatic textural evolution might be revealed.

While the ultimate goal of this research is to evaluate the significance of grain boundary migration using new experimental techniques, this thesis addresses important intermediary steps towards this goal. For the purpose of this thesis: (1) the ability of a synthetic binary solid solution to model igneous textural evolution was evaluated, and (2) experiments were designed in which the crystallization of a synthetic binary solid solution would record the process of grain boundary migration.

1.2 Background: (1) High temperature laboratory crystallization of feldspars

Many crystallization experiments have been conducted for the purpose of investigating magmatic phase relations (e.g. Bowen, 1913), but the works of Lofgren (1974), Kirkpatrick, *et al*. (1979), and Muncill and Lasaga (1988) stand out in the use of high temperature experiments to investigate the development of plutonic igneous textures involving feldspars.

Lofgren (1974) used an internally heated pressure vessel to investigate the development of plagioclase crystal morphology under isothermal conditions. Experiments were conducted at 5 kb water pressure and at temperatures between 500 and 1200 °C; plagioclase compositions between 0 and 25% anorthite were tested. In the experiments, samples were rapidly cooled to a predetermined temperature below the liquidus. Crystallization was allowed to proceed for 1 to 3 days; samples were then quenched to 100 °C within 7 minutes. Undercoolings of 100 to 150 °C produced a variety of crystal morphologies from equant (least amount of undercooling) to acicular, skeletal, dendritic, and spherulitic (greatest amount of undercooling). The transition from one type of morphology to another was gradual, and sequential crystal forms often occurred together. Lofgren explained his results in terms of the ratio between the diffusion coefficient of components rejected during growth (D), and growth rate (G). When D/G approached or exceeded 1, for example, plagioclase crystals appeared tabular.

When D/G became much less than 1, plagioclase crystal morphology approached the spherulitic form.

In 1979, Kirkpatrick *et al.* introduced the technique of plagioclase crystal growth using a microscope heating stage. Crystals with compositions of $An_{75}Ab_{25}$ and $An_{50}Ab_{50}$ were observed and photographed during growth (with a motion picture camera) at temperatures near the liquidus in an argon atmosphere. Crystal morphology, growth rate, and attachment kinetics were studied during the experiments. Undercoolings of less than 40 °C in crystals of An_{75} composition produced faceted, euhedral crystals; undercoolings of 40 and 50 °C produced crystals with skeletal morphology; undercoolings of 50 to 100 °C produced dendritic, spherulitic or fibrillar (needle-like crystals radiating from the surface of the sample) crystals. The crystal morphologies observed with the microscope heating stage were similar those created by Lofgren in 1974. In general, growth rates were observed to increase with increasing undercoolings below the liquidus until a maximum was reached; growth rates would then decrease with increasing undercoolings. The development of impingement relationships were observed but not studied; they were considered an impediment to the measurement of true growth rates.

In 1983, Tsukamoto and Sunagawa observed the crystallization of anorthite and diopside using a high temperature (up to 1527 °C) growth cell. Crystal growth mechanisms were examined; both layer growth and surface roughening were observed to take place during the growth of a single crystal.

Using an internally heated pressure vessel, Muncill and Lasaga (1988) explored the kinetics of crystal growth within the plagioclase binary solid solution. Plagioclase crystals (An_{30} and An_{10}) were grown at 2 and 5 kbar at temperatures between 550° and

1100 °C. Experiments were conducted with the purpose of examining the mechanisms of crystal growth, and determining rate-controlling factors. They formed the following conclusions about plagioclase growth rates: (1) at small degrees of undercooling, crystal-melt interface reactions were the primary rate controlling processes, and (2) at high degrees of undercooling, the kinetics of advective and diffusive mass transfer were the primary processes controlling growth rate.

Experiments using pressure vessels can be conducted within large temperature and pressure ranges similar to those within a magma chamber, but they do not allow the observation of paths of crystallization. Processes like grain and phase boundary migration may take place but cannot be studied. While experiments conducted by Kirkpatrick *et al.* (1979) used a microscope heating stage, and Tsukamoto and Sunagawa (1983) used a high temperature growth cell to observe crystallization, textures characteristic of large igneous plutons were not targeted products.

1.3 Background: (2) synthetic crystallization experiments

Crystallization experiments using synthetic materials with low melting points can circumvent the "black box" problem of high-temperature vessel experiments and allow *in situ* observation of crystallization processes. In addition, the textural evolution of a low-temperature synthetic system can be studied using a petrographic microscope (e.g. Tsukamoto, 1983; Means and Park, 1994). Experiments using synthetic organic materials will differ from those using silicates, however, and caution must be exercised when drawing conclusions about natural systems from the synthetic system data.

Means and Park (1994) used the synthetic compounds ammonium thiocyanate, ammonium chloride, and diammonia tetrathiocyanatocobaltate to create a three-component, eutectic system in which the solid phases crystallized below 100 °C. Solid phases were crystallized from an aqueous solution and resulted in textures similar to plutonic cumulates, and paths of crystallization were observed *in situ* with a petrographic microscope. Using this new synthetic system, grain boundary migration was observed between two crystals of NH_4SCN. An example of textures produced by Means and Park (1994) is shown in Figure 3.

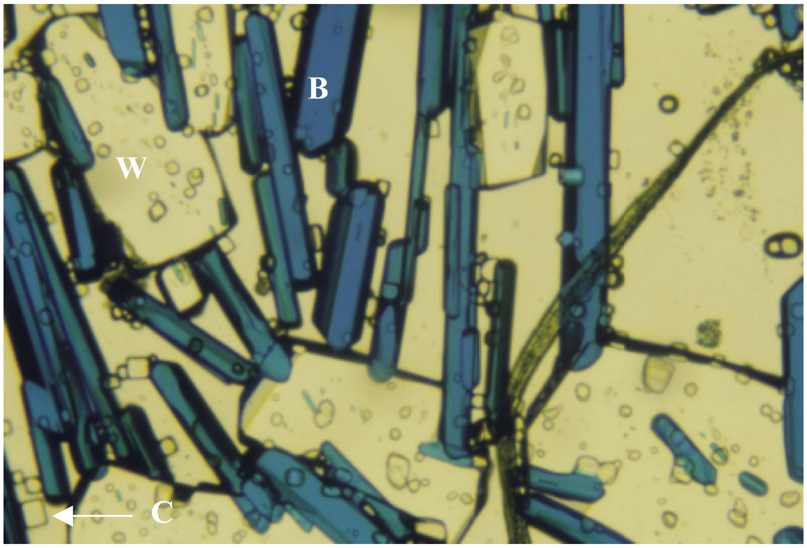

Figure 3. Three-component system created by Means and Park (1994). The system includes a white (W) phase (NH_4SCN); cube (C) phase (NH_4Cl); and blue (B) phase $(NH_4)_2[Co(SCN)_4] \cdot nH_20$.

Chapter 2

Mineralogy and Crystal Chemistry

Plagioclase Solid Solution

Potassium – Ammonium Thiocyanate Solid Solution

Morphology, crystallography, crystal chemistry, optics, and phase relations are attributes that may affect grain-to-grain interactions, or the manner in which final textures are observed. In order to facilitate a direct comparison between plagioclase and (K, NH_4)SCN, characteristics common to plutonic plagioclase are first discussed, and then those of the (K, NH_4)SCN solid solution. There are many striking similarities between plagioclase and the thiocyanates — particularly in morphology and twinning. Thiocyanate compounds are not silicates, however, and the implications of this difference are discussed at the end of the chapter.

2.1 Plagioclase: Albite ($NaAlSi_3O_8$) – Anorthite ($CaAl_2Si_2O_8$)

2.1a Morphology

The development of plutonic textures near equilibrium may be largely controlled by surface energy minimization (Hunter, 1987). For this reason, similarities in crystal morphology between plagioclase and a synthetic analogue may be important in determining the efficacy of the analogue.

When isolated plagioclase crystals grow unrestricted within a melt near equilibrium, they form crystalline laths elongated in the c direction (Figure 4 A; Lofgren, 1974). This type of crystal morphology is characteristic of development within large igneous plutons.

Differences in cooling rate and nucleation characteristics, however, can produce plagioclase crystals with a wide range of morphologies. Laboratory experiments have produced skeletal, fibrilar, spherulitic, and dendritic plagioclase crystals by crystallizing silicate material at temperatures 40 to 200 °C below the solidus (Lofgren, 1974; Kirkpatrick, *et al.*, 1979; Muncill and Lasaga, 1988).

Igneous plagioclase crystals are commonly twinned (Figure 4 B, C). Pericline and Carlsbad twins are specifically found in intermediate and calcic compositions of plagioclase while albite twins are common in all compositions (Nesse, 1991).

2.1b Plagioclase crystallography

Table I: Plagioclase symmetry elements[1], and unit cell parameters[2].

Crystal system		Triclinic		
Crystal class		$\bar{1}$		
Albite space group		C $\bar{1}$		
Anorthite space group		P $\bar{1}$		
Unit cell parameters	a (Å)	b (Å)	c (Å)	β
Albite	18.14	12.8	7.16	116.4
Anorthite	8.18	12.87	7.08	115.8

[1] Ribbe, 1983
[2] Kroll, 1983

During the cooling of plagioclase feldspars, exsolution and ordering processes create finely inter-grown atomic microstructures that effectively prevent good resolution of the plagioclase unit cell by x-ray diffraction (Kroll, 1983). While anorthite has a unit cell in which c ~14 Å and albite has a unit cell in which c ~ 7 Å (Figure 5), the similar d_{hkl} – spacings of anorthite and albite render it impossible to resolve the Al and Si distributions

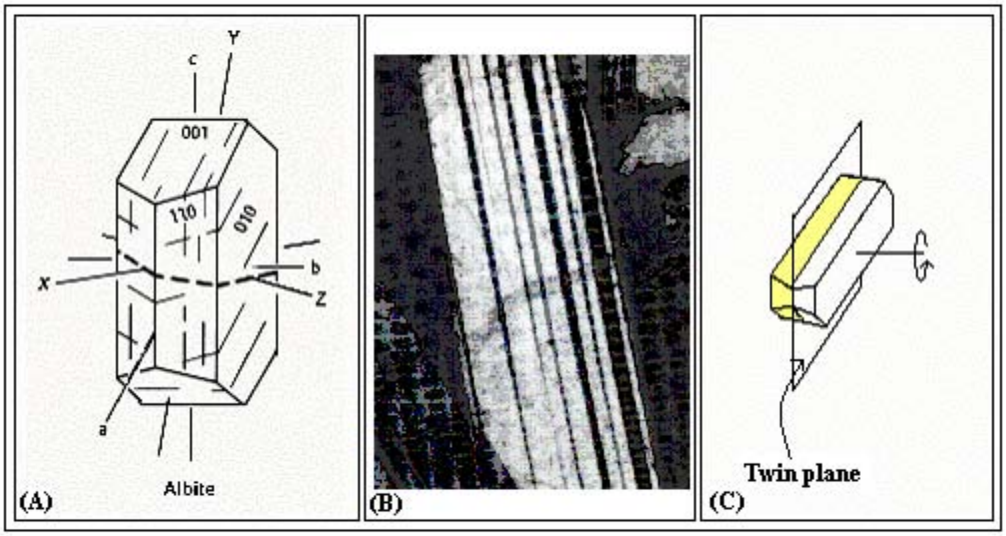

Figure 4. Albite morphology and twinning. (A) Albite crystallographic axes (a, b, c), optic axes (X, Y, Z), and crystal forms (after Nesse, 1991). (B) Photomicrograph of plagioclase with polysynthetic albite twins; cross polarized light (From Nesse, 1991). (C) Illustration of the albite twin law (After Blackburn and Dennen, 1994).

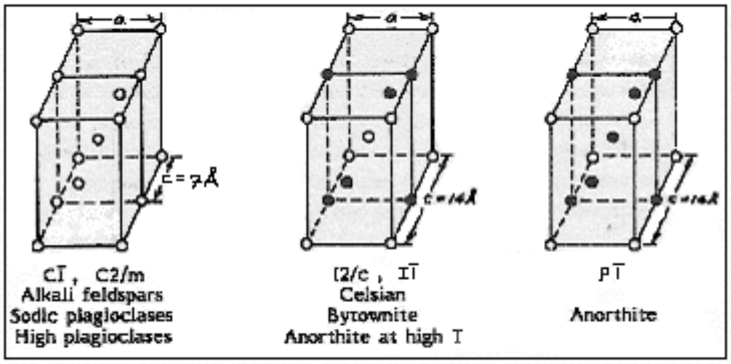

Fig. 5. Principal feldspar lattice structures. The open circles represent lattice points and the filled circles represent pseudo-lattice points. The unit cells vary from c = 7 Å to c = 14 Å, (From Ribbe, 1983).

in calcic plagioclase with a c ~ 14 Å cell and $P\bar{1}$ space group; (Ribbe, 1983). However, bulk crystals can be analyzed in such a way that structural and compositional variations are taken into account for the determination of an average unit cell in which c = 7 Å, (Kroll, 1983). Parameters describing the average structures of albite and anorthite are presented in Table 1.

2.1c Crystal chemistry

The feldspar crystallographic structure is characterized by a “crank-shaft” formation (Figure 6) in which corner-sharing AlO_4 and SiO_4 tetrahedra are infinitely linked (Ribbe, 1983). AT_4O_8 generally describes the feldspar chemical formula; “A” represents monovalent or divalent cations with radii greater than 1 Å, and “T” represents Al or Si. The A cations occupy large spaces within the tetrahedral framework and include: Ca, Ba (alkaline-earth feldspars); Na, K (alkali feldspars); K, Ba (hyalophanes); Na, Ca (plagioclase feldspar series). The A polyhedral sites can also contain trace amounts of Sr^{2+}, Rb^{+}, Cs^{+}, Pb^{2+}, Fe^{2+}, and even NH_4^{+} (Ribbe, 1983).

The feldspar crystal structure is noticeably affected by the size of the cation occupying the A site. Celsian ($BaAl_2Si_2O_8$), for example, incorporates a large Ba cation with a radius of 1.4 Å and a unit cell defined by c ~ 14 Å with a high degree of symmetry. In contrast, anorthite incorporates the smaller Ca cation into its framework. Although it has a unit cell also defined by c ~ 14 Å, the smaller ionic size results in a partially collapsed framework (Figure 7) and a loss of symmetry (Ribbe, 1983).

Feldspars with an Al:Si ratio of 1:1 (i.e. anorthite) have a general formula of $A^{2+}Al_2Si_2O_8$. In order to maintain a neutral charge balance, Al and Si distribute within

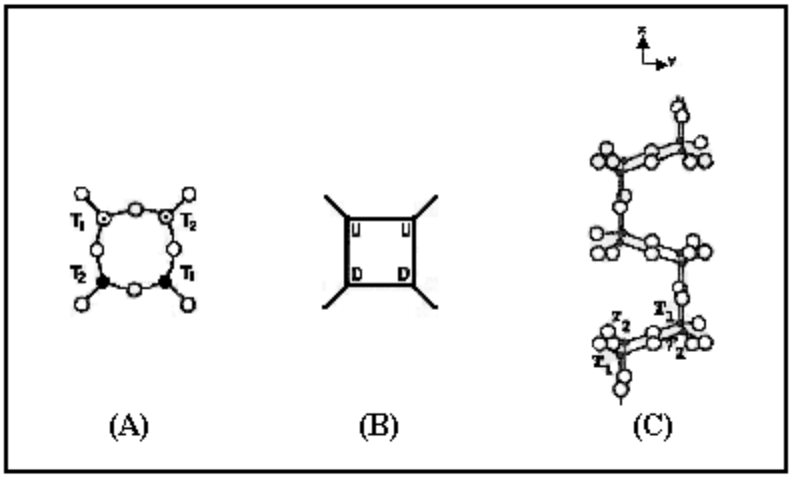

Figure 6. In all feldspars, four-membered tetrahedral rings are arranged in a double-crankshaft structure that runs parallel to *a*. (A) Four silicon-oxygen tetrahedra arranged in a ring; (B) Stylized version of the four-membered ring in which "U" indicates an upward-pointing tetrahedron, and "D" indicates a downward-pointing tetrahedron,. (C) The four-membered tetrahedral rings are arranged in a double-crankshaft chain that is characteristic of all feldspars (After Ribbe, 1983).

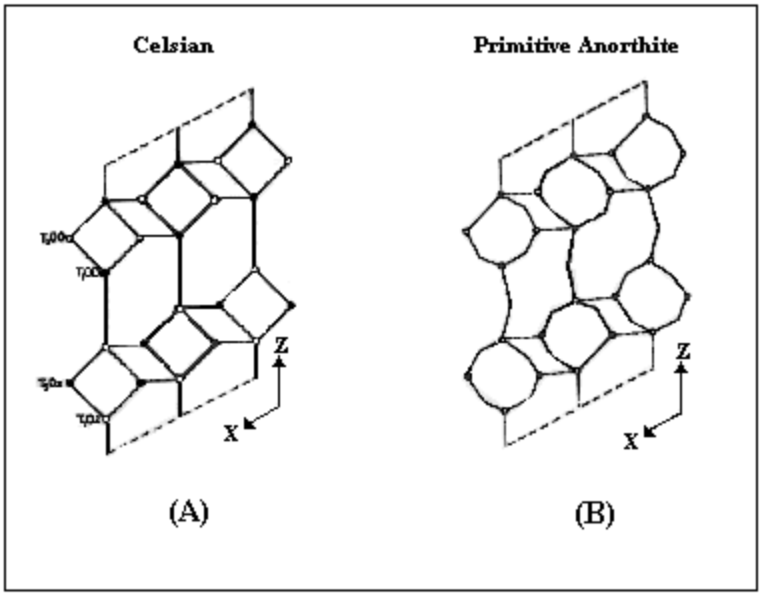

Figure 7. The Al-Si ordering pattern is the same in both celsian and anorthite, but the small size of the Ca cation in anorthite (compared to Ba in celsian) causes it to have a partially collapsed framework. Open circles represent Al and dots represent Si. (A) Celsian crystal structure. (B) Primitive anorthite crystal structure.

the framework according to the aluminum avoidance principle (Loewenstein, 1954). Due to the apparent instability of Al-O-Al linkages, Al and Si tetrahedra remain isolated; Al tetrahedra are surrounded by Si tetrahedra, and vice versa, (Ribbe 1983). As a result, Al and Si do not diffuse easily within the plagioclase crystal structure — a fact that helps explain the abundance of metastable plagioclase structures such as peristerite intergrowths (Kroll, 1983).

2.1d Optics

In plane polarized light, plagioclase crystals appear colorless and have low (positive or negative) relief relative to quartz (or thin-section epoxy). Plagioclase refractive index systematically increases with increasing anorthite content and can be used to determine composition (within 2%), (Chayes, 1952). In cross polarized light, maximum interference colors of crystals 30 μ m thick appear first order gray to white (most compositions) or first order yellow for extremely calcic plagioclase. Birefringence (albite ~ 0.007; anorthite ~ 0.013) and 2V vary systematically with anorthite content, but do not provide the resolution needed for accurate compositional determination (Nesse, 1991).

Elongate plagioclase crystals exhibit oblique extinction, and extinction angle is commonly used to determine composition (although results are less accurate than those from refractive index techniques), (Noble, 1965). Two of the most common methods for determining composition from extinction angles include the Michel-Levy method and the Carlsbad-albite method. In the Michel-Levy method, polysynthetically twinned plagioclase crystals are oriented so that the (010) composition plane is vertical. In this orientation, both composition and indicatrix position can control the observed extinction angle; thus, several grains are measured and the maximum angle obtained is compared to a chart correlating extinction angle with composition.

The Carlsbad-albite method is similar to the Michel-Levy method; albite extinction angles are measured in both Carlsbad twins and then compared to a chart that correlates composition with extinction angle. Using this method, only one grain with the proper orientation is needed to determine anorthite composition (Nesse, 1991).

2.1e Chemical zoning

Zoning patterns in plagioclase crystals are optically visible, and a large variety of patterns have been observed. Plagioclase crystals with the following zoning patterns have been described in rocks of plutonic and/or volcanic origin: (1) normal or reverse (normal refers to crystals with an An-rich core and Ab-rich rim, while reverse refers to the opposite compositional trend); (2) continuous or discontinuous (continuously zoned plagioclase crystals exhibit a smooth transition in composition from core to rim, while discontinuously zoned crystals contain abrupt changes in composition); (3) sector (hour-glass zoning pattern) (4) oscillatory zoning (discontinuous, repeated changes in composition), and (5) convolute zoning (erratic patterns with non-uniform thickness), (MacKenzie *et al.*, 1991). Some crystals can also be described as concentrically zoned; layers of compositional uniformity give the appearance of euhedral, concentric growth and provide a textural history of crystal growth (Pearce and Kolisnik, 1989). In Figure 8, an anhedral crystal of plagioclase is concentrically zoned indicating a euhedral growth history (Hibbard, 1995).

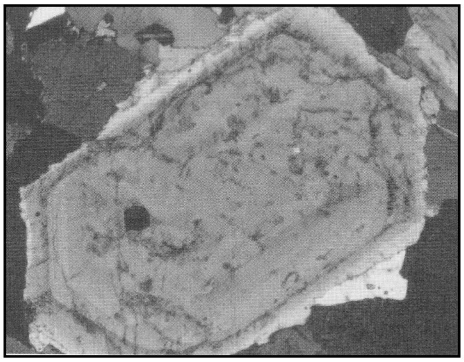

Fig. 8. Concentric zoning of an anhedral crystal indicates prior euhedral growth (from Hibbard, 1995).

2.1f Liquidus phase relations

Plagioclase forms a binary solid solution between $NaAlSi_3O_8$ (albite) and $CaAl_2Si_2O_8$ (anorthite) in which Na^+ and Ca^{2+} can substitute within the plagioclase crystal structure. $NaAlSi_3O_8$, and $CaAl_2Si_2O_8$ melt at 1,100 and 1,550 °C respectively (Bowen, 1913), and plagioclase crystals of intermediate composition melt over a range of temperatures between these two values. Figure 9 illustrates a phase diagram constructed for the albite-anorthite (plagioclase) system.

Large, igneous plutons take millions of years to crystallize—a fact that often makes the assumption of equilibrium conditions practical (e.g. Smith, 1983; Hunter, 1987) in the investigation of plagioclase phase relations. Equilibrium, defined by $\Delta G = 0$, is a thermodynamic condition in which the free energy change of a system is equal to zero. Temperature and pressure are constant at equilibrium, causing a crystal mush to crystallize and melt binary solid solution components at the same time. Net changes in crystal/melt volume do not take place, only crystals stable at a given temperature and pressure are present. The phase diagram presented in Figure 9 includes equilibrium phase relations for the system $NaAlSi_3O_8$ (Albite) – $CaAl_2Si_2O_8$ (Anorthite).

In order to explain chemical zoning patterns characteristic of plutonic plagioclase, a revised model of equilibrium — or "local equilibrium" — is applied to the binary solid solution model (Thompson, 1959). This model of plutonic development recognizes that, while a large ΔT is required to crystallize a pluton over millions of years, the effective ΔT at any single point in time (even days or years) is effectively zero. Each molecular addition to a plagioclase crystal is effectively in equilibrium with the available melt, and its chemical composition is determined by the temperature, pressure, and chemical

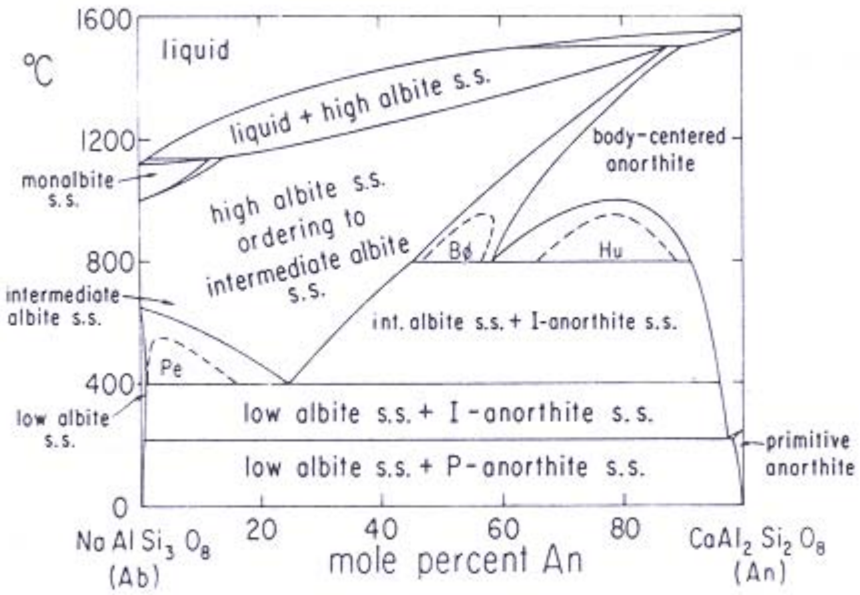

Figure 9. Equilibrium phase diagram for the system $NaAlSi_3O_8$ (Albite) – $CaAl_2Si_2O_8$ (Anorthite) at constant pressure. The dashed lines represent metastable phase boundaries, (from Smith, 1983).

composition of the melt at that time. However, when the temperature of a pluton drops, molecular layers may become chemically isolated and unable to react with melt, causing a change in the chemical composition of the melt. The next plagioclase layers to form will be in equilibrium with the new melt composition, and are chemically distinct from the previous molecular layers.

Crystals produced by the complete crystallization of a pluton containing plagioclase binary solid solution components will not be uniform in composition. Instead, they will change composition from core to the rim and form normally zoned plagioclase crystals. These crystals characteristically decrease in calcium content from core to the rim, and increase in sodium content from core to rim. The net result is a reflection of crystallization under disequilibrium conditions.

2.1g Sub-solidus phase relations

Thermal history is a determining factor in the formation of zoned crystals (as described above), as well as crystal structure. The phase diagram presented in Figure 9 illustrates a model in which the stable assemblage of low albite and P-anorthite is the final assemblage of all plagioclase feldspars under equilibrium conditions (Smith, 1983). All other plagioclase structures are relicts of high temperature conditions, preserved by kinetic barriers, (Smith, 1983). Structural changes in the plagioclase feldspar system can take place by diffusive polymorphic transitions (e.g. from monalbite to high albite) or by displacive polymorphic transitions (e.g. from body-centered (I) anorthite to primitive (P) anorthite). The re-ordering of Al and Si within the feldspar crystallographic framework results in the formation of a glide plane and can take place because of anorthite pseudosymmetry (Ribbe, 1983)

2.2 (K, NH$_4$)SCN Solid Solution

2.2a Morphology

Synthetic crystals produced by the (K, NH$_4$)SCN solid solution form crystalline laths elongated in the c direction. Aspect ratios vary with composition and range from 1:2 (NH$_4$SCN) to > 1:10 (KSCN). Ammonium thiocyanate (Figure 10) can undergo transformation twinning (Means, 1992), and crystals containing K within the (K, NH$_4$)SCN solid solution have also been observed (in this study) to polysynthetically twin.

2.2b Crystallography

Table II: (K, NH$_4$)SCN symmetry elements and unit cell parameters

	System	Space group		
KSCN (room temp.)	Orthorhombic[1]	Pbcm*		
NH$_4$SCN (room temp.)	Monoclinic[1]	P2$_1$ /c**		
Unit cell	a(Å)	b(Å)	c(Å)	β
[2]KSCN (room temp.)	6.7	6.6	7.6	-
[3]NH$_4$SCN (22 ˚C)	4	7	13	97.8˚

[1] Smirnov *et al.*, 1994
[2] Klug, 1933; Yamada and Watanabé, 1963
[3] Klement and Pistorius, 1976
* Akers *et al.*, 1967
** Bats and Coppens, 1977

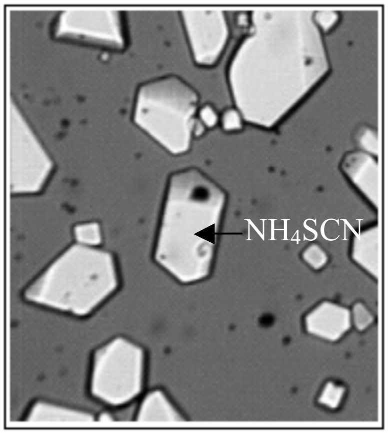

Figure 10. Microphotograph of NH$_4$SCN and melt in plane polarized light (Courtesy of Dr. W. Means).

The unit cell parameters of the pure end-members KSCN and NH_4SCN differ slightly at room temperature. At 17 °C, KSCN is orthorhombic while NH_4SCN is monoclinic with a beta angle of ~78°. As temperature increases, the unit cell volumes of compounds within the (K, NH_4)SCN solid solution also increase (Smirnov, 1994). Data on the variation of cell parameters and volumes with temperature and composition, acquired in a neutron diffraction study by Smirnov et al. (1994), are presented in Figure 11.

2.2c Crystal chemistry

The SCN^-anion is essentially linear with S and C linked by a single bond, and C and N linked by a triple bond (Akers *et al.*, 1967). K^+ and NH_4^+ have similar Pauling radii — 1.48 Å and 1.33 Å respectively, and the contribution of charge by the NH_4^+ cation to the SCN^-anion is 0.5 to 0.6 e (a value of 1.0 represents a pure ionic model, Akers *et al.*, 1967). The charge contribution of the K^+ cation, however, is not known. KSCN and NH_4SCN have similar crystal structures (Klement, 1976) and Figure 12 includes a stereoscopic view of the NH_4SCN crystal structure.

2.2d Optics

In thin-section, ammonium and potassium thiocyanate crystals are colorless in plane polarized light and interference colors range from extreme white (NH_4SCN) to third-order (KSCN) in samples created for use in synthetic experiments. The large range in retardation is due to variations in thickness and birefringence.

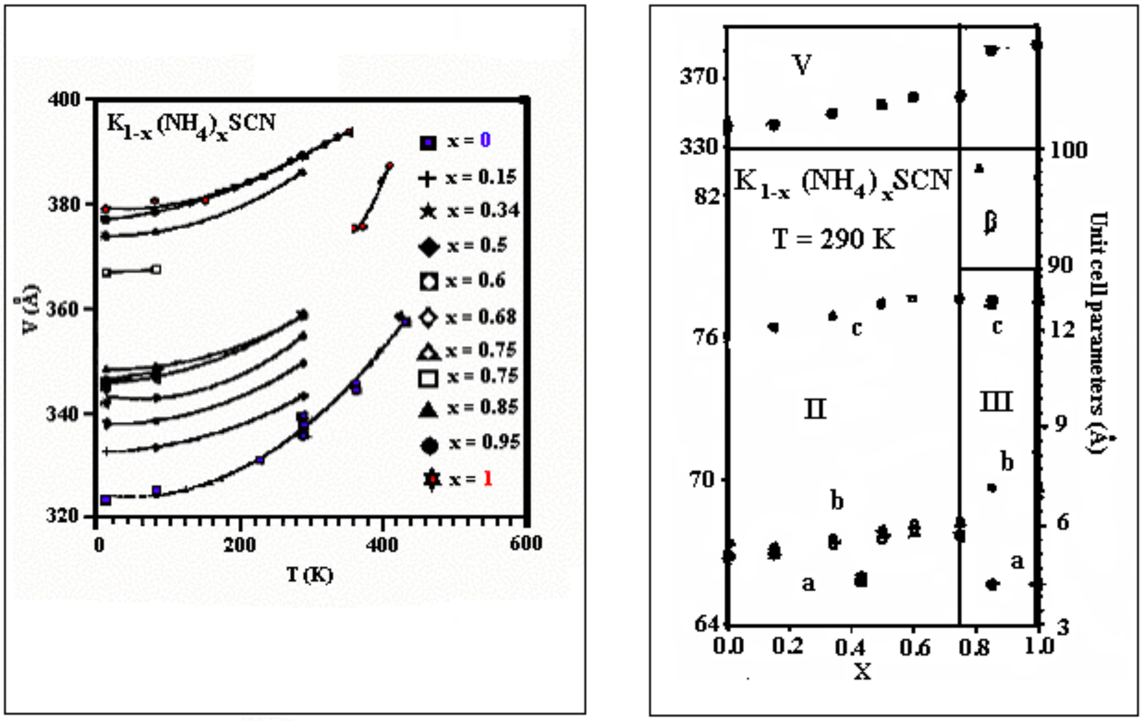

(A) (B)

Figure 11. (A) Plot demonstrates the effect of temperature on unit cell volume for several compositions within the (K, NH$_4$)SCN solid solution. (B) Illustrates the differences in unit cell parameters a, b, c, and β for various compositions within the (K, NH$_4$)SCN solid solution, (Smirnov *et al*., 1994).

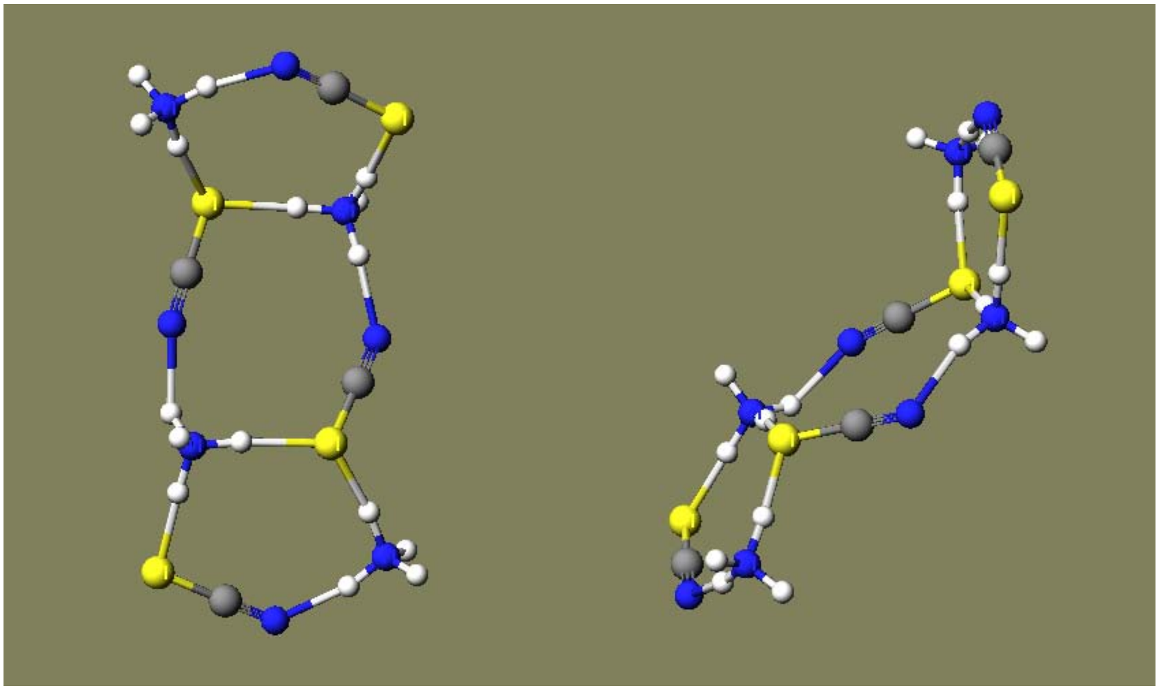

Fig. 12. Representation of the NH_4SCN crystal structure (two orientations) in which blue spheres represent N, gray spheres represent C, yellow spheres represent S, and white spheres represent H. (Courtesy of Ian Scott; based upon data from Bats and Coppens, 1976).

The optical relief of ammonium and potassium thiocyanate is high, but changes considerably under plane polarized light depending upon orientation. Figure 13 (A, B, and C) includes three photographs: (A) crystals of pure KSCN with third order interference colors in an aqueous solution (black), (B) crystals of pure NH_4SCN with extreme white interference colors, and (C) crystals with third order interference colors formed by the $(K, NH_4)SCN$ solid solution.

2.2e Phase relations

Mixtures of KSCN and NH_4SCN form a binary solid solution; pure KSCN and NH_4SCN melt at 172.3 and 149.6 °C respectively (Alfa Aesar) and crystals of intermediate composition hypothetically melt over a range of temperatures between these two values (Figure 14). The $(K, NH_4)SCN$ solid solution is continuous for all compositions between pure KSCN and pure NH_4SCN at temperatures above –193 °C (Smirnov *et al.*, 1994). $(K, NH_4)SCN$ solid solutions undergo solid-solid phase transitions from tetragonal (just below the liquidus) to orthorhombic with decreasing temperature. Ammonium-rich compounds make a second transition from orthorhombic to monoclinic at ~ 85 °C. Below –193 °C, a solvus exists; crystals of mixed composition between KSCN and NH_4SCN can occur in monoclinic and orthorhombic phases.

The phase diagram of $(K, NH_4)SCN$ phase relations (Figure 14) is constructed from melting points provided by Alfa Aesar, and phase transition data from Smirnov *et al.* (1994). If a sample within the $(K, NH_4)SCN$ solid solution has a molar composition of $(X_K) = 0.75$, and is held at a temperature of 0 °C, (represented on the diagram by an “a”) it will theoretically occur in orthorhombic crystalline form. If this sample is

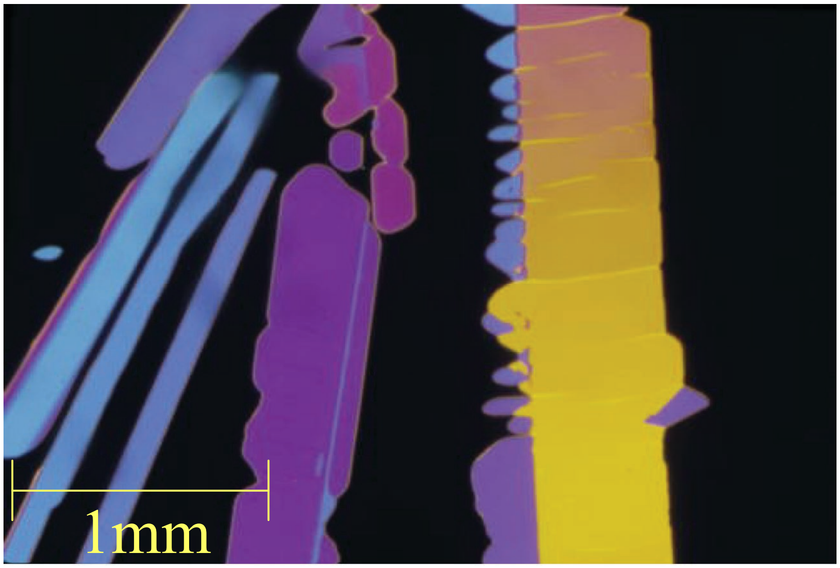

Figure 13A. Microphotograph of crystals of KSCN under cross polarized light. Black areas include melt and extinct crystals.

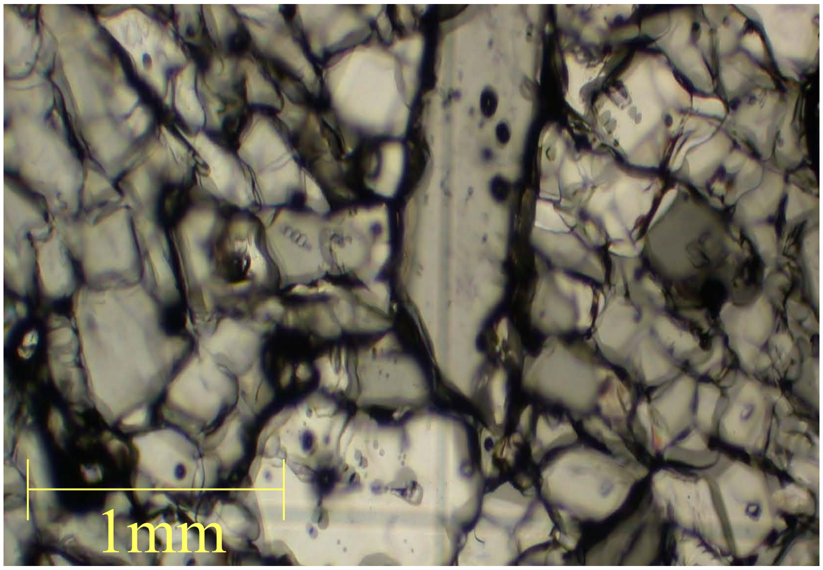

Figure 13B. Microphotograph of crystals of NH_4SCN showing extreme white interference colors.

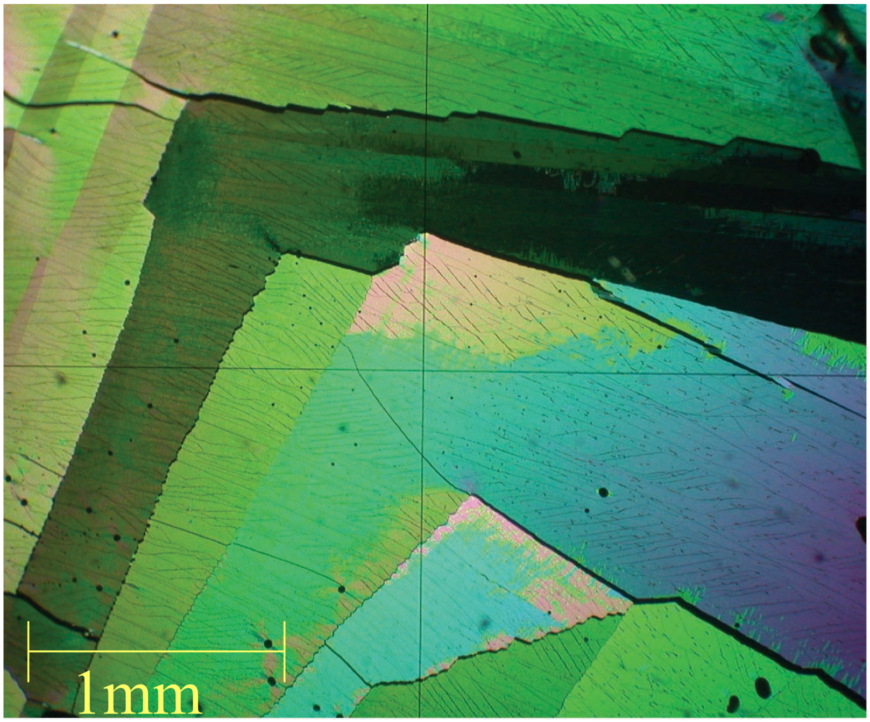

Figure 13C. Photomicrograph of crystals of (K, NH_4)SCN solid solution, with composition $X_K = 0.80$, under cross polarized light.

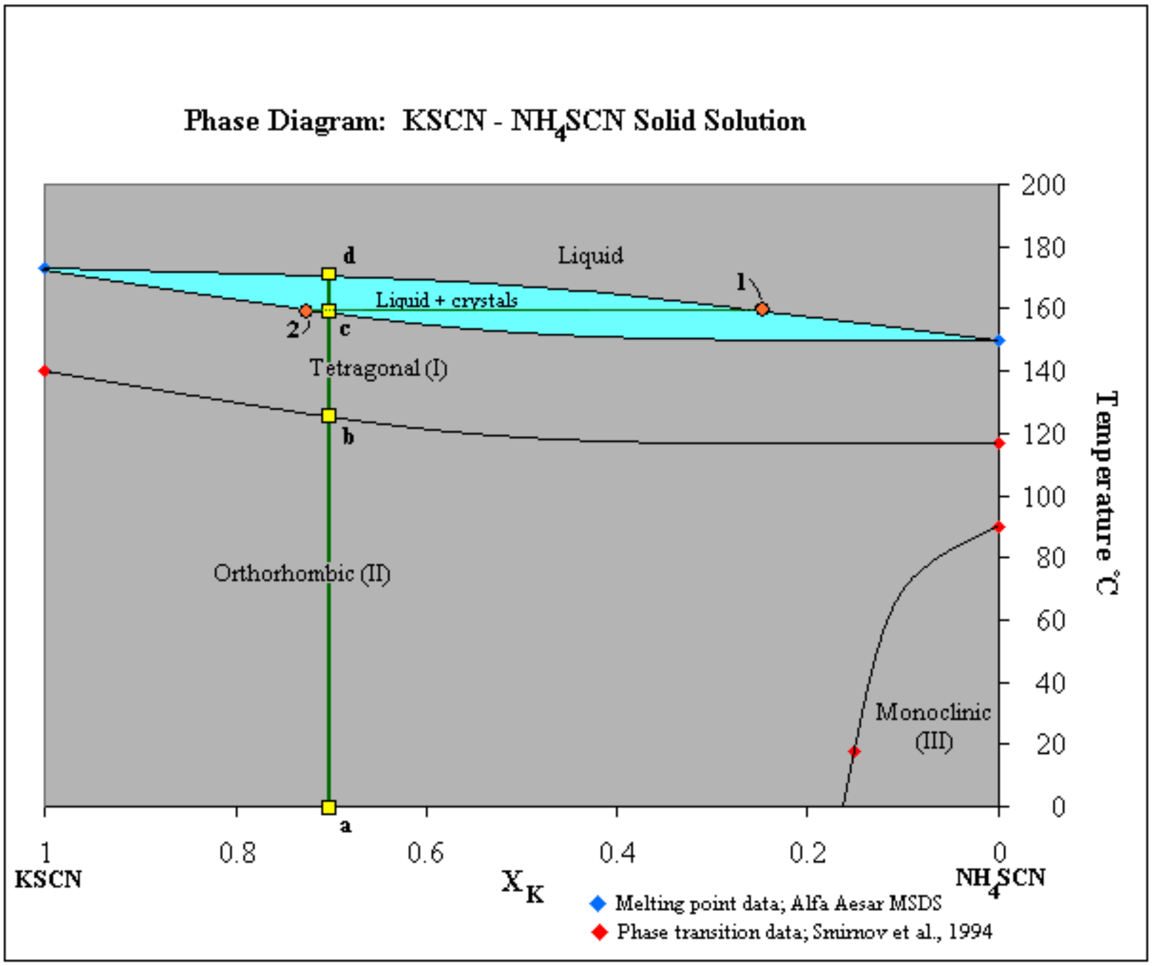

Figure 14. Phase diagram constructed from melting point data (Alfa Aesar) and phase transition data (Smirnov *et al*., 1994).

heated until it reaches position “b”, then it will undergo a solid-solid phase transition from orthorhombic (II) to tetragonal (I). The composition of the crystals will remain the same and reflect the starting composition. With continued heating to position “c”, the crystals will begin to melt. At this point, the first melt to form will have a composition more ammonium-rich than the original solid (represented by marker “1”), and the remaining crystals will be more potassium-rich (represented by marker “2”). As heat to the system is added, the melt composition will move up the liquidus, and the composition of the crystals will move up the solidus until the melt composition reaches the same composition as the original crystalline starting material (position “d”).

Solid-phase transitions of compounds within the (K, NH_4)SCN solid solution result in the ordering of ions with decreasing temperature. The transition from tetragonal to orthorhombic KSCN, for example, is due to the ordering of SCN ions. An analogous transition in NH_4SCN is due to the ordering of SCN and two NH_4 ions; another two NH_4 ions are ordered during the transition from orthorhombic to monoclinic, (Smirnov *et al.*, 1994). Figure 15 illustrates the ordering of SCN ions in KSCN.

2.3 Comparison between plagioclase and its (K, NH_4)SCN analogue

The plagioclase binary solid solution produces crystalline laths elongated in the c direction (Lofgren, 1974) with aspect ratios of ~ 1:1.6. Maximum interference colors range from first order gray to first order yellow for crystals 30 μm thick (Nesse, 1991), and extinction angle varies systematically with composition (Noble, 1965). Plagioclase polymerizes during crystallization and incorporates corner-sharing AlO_4 and SiO_4 tetrahedra into a characteristic “crank shaft” crystal structure (Ribbe, 1983). Ionic bonds

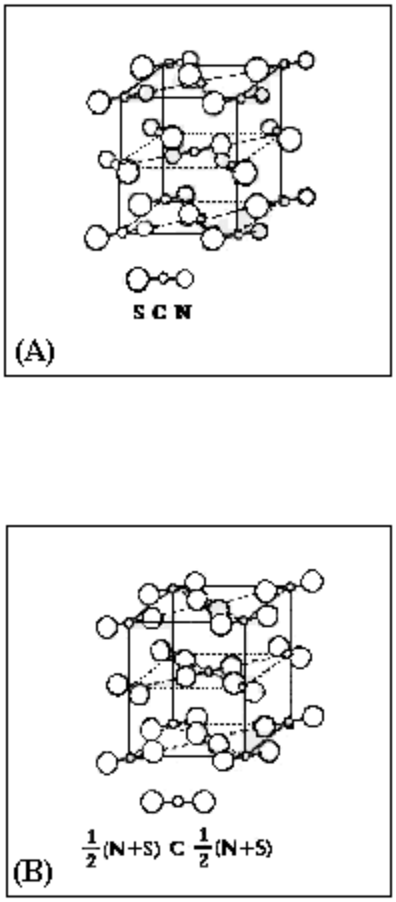

Figure 15. SCN ordering (in KSCN) is temperature dependent and causes volume changes near the phase transition temperature: (A) Thiocyanate ions (S, C, N) in a room temperature arrangement; (B) Thiocyanate ions (S, C, N) in a high temperature (160 °C) arrangement (From Yasusada and Watanabe, 1963).

between the Al - Si tetrahedra and Ca^{2+} or Na^{+} cations make coupled substitution and chemical zoning possible.

The (K, NH_4)SCN solid solution produces crystalline laths elongated in the c direction with aspect ratios of ~ 1:2. Maximum interference colors range from extreme white (greater than fifth order) to third order, with a large range in retardation due to variations in thickness and birefringence. Ionic bonding between monovalent cations (K^{+} and NH_4^{+}) and the SCN^{-} anion make substitution and chemical zoning possible. The (K, NH_4)SCN solid solution does not require coupled substitution to maintain a neutral charge balance.

In order for a plagioclase analogue to provide useful information about plutonic textural evolution, similarities in morphology, chemical bonding, substitution, and chemical zoning are necessary. Crystals produced by the (K, NH_4)SCN solid solution generally satisfy these requirements: the synthetic crystals are similar in morphology to those of plagioclase and have similar aspect ratios; ionic bonding enables the process of substitution and the formation of a solid solution.

One significant difference between plagioclase and (K, NH_4)SCN melts is the ability of the silicate melt to polymerize and form Si – O – Si bonds. Polymerization is a controlling factor in the rates of nucleation; less polymerized material nucleates more quickly than more polymerized material (Kirkpatrick, 1983). As such, the (K, NH_4)SCN synthetic system is not a good system with which to study nucleation rates in silicate melts. However, the lack of polymerization within crystals or melt generated by the (K, NH_4)SCN solid solution should not affect the ability of the analogue to texturally evolve in a manner similar to plagioclase.

Chapter 3

Experimental Design

3.1 Apparatus

A stage heater apparatus was designed and developed for the purpose of conducting low temperature crystallization experiments. The apparatus was constructed to heat and cool synthetic compounds (within a range of 25 to 200 °C) so that crystallization processes could be optically analyzed and digitally photographed *in situ*. The stage heater apparatus contains: (1) a Eurotherm 847 temperature controller, (2) a chromel-alumel thermocouple, (3) an Omega circular heater, (4) a custom-built, gold-plated, brass stage heater, (5) a Leitz Wetzlar polarizing microscope, (6) a Nikon Coolpix 995 digital camera, (7) a Dell PC, and (8) Photo PC software. A diagram of the primary constituents is illustrated in Figure 16. The Nikon camera was specifically chosen because of an exact fit between the screw mounting of the camera lens and that of the microscope eyepiece.

The Eurotherm 847 was used to control the temperature of the stage heater. The user interface allowed a temperature to be selected as a target temperature, while displaying the current temperature of the stage heater. The tip of the chromel/alumel thermocouple was placed on top of a sample slide, and the temperature information it generated was used by the Eurotherm to adjust the temperature by supplying power to the Omega heater. The Omega heater surrounded a round stage heater (Figure 17); the round shape of the stage heater was used to produce uniform temperatures. The stage heater was machined from brass and plated with gold (to reduce reactivity with sample material and

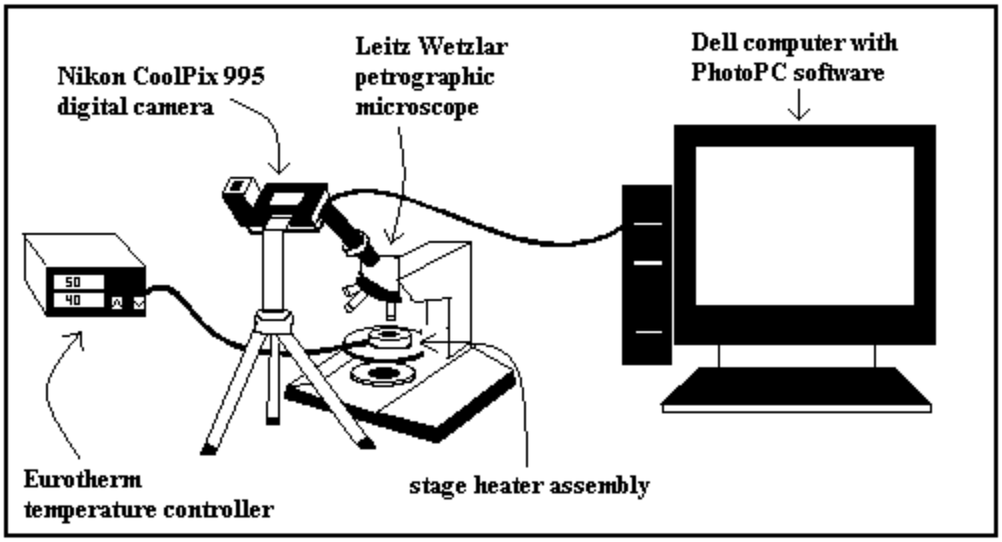

Figure 16. Diagram of the stage heater apparatus including: temperature controller, digital camera, polarizing microscope, stage heater assembly, and computer.

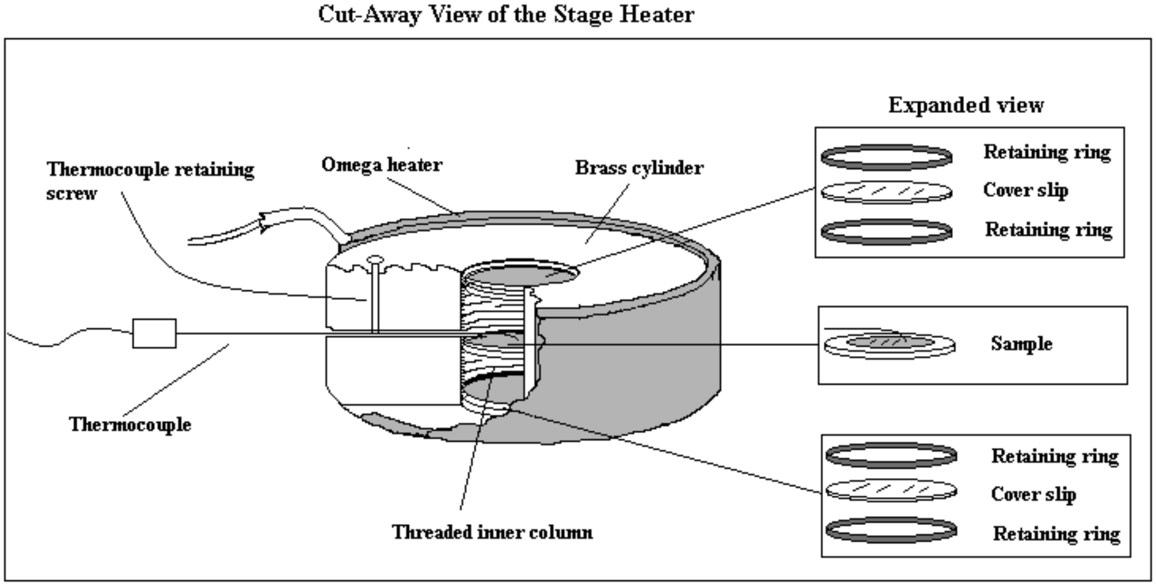

Figure 17. The stage heater assembly, including: thermocouple, thermocouple retaining screw, heater, brass cylinder, threaded inner column, cover slips, retaining rings, and sample.

small inside lip. The upper and lower portions of the inner hollow area were threaded so that small rings could be threaded inside in order to support plain glass cover slips to reduce temperature gradients and allow the optical observation of samples.

The heating apparatus was placed on the stage of a Leitz Wetzlar polarizing microscope, and the optical lens of the camera was positioned over the eyepiece and snugly screwed in place. The camera was linked to a Dell Dimension 8200 PC. In turn, a batch file was created using the Nikon CoolPix source code, enabling the camera to be completely controlled by the PC (and the user). Using this system, experiments were run in which crystallization processes took place in thin section and were digitally photographed at predetermined intervals using the PC's task manager to run the camera-controlling batch file. The result was a partially automated system for running synthetic crystallization experiments in which the paths of crystallization were photographed at regular intervals.

3.2 Designing a synthetic igneous analog capable of solid solution

Ammonium thiocyanate (introduced as an igneous analogue by Means and Park, 1994) was chosen as a potential solid solution end-member for the following reasons: (1) the ionic nature of ammonium-thiocyanate bonds meant that another ion might substitute for the ammonium cation and form a solid solution, (2) ammonium thiocyanate has a relatively low melting point of 149.6 °C, a temperature that would not damage petrographic equipment, (3) crystals of ammonium thiocyanate and plagioclase have similar morphology.

In order for another ion to substitute for NH_4^+ within the thiocyanate crystal structure, two necessary conditions needed to be met. First, the ionic radius of a substitute needed to differ from the original by less than fifteen percent. Second, the two ions needed to have the same charge in order to maintain electrical neutrality (Faure, 1998). Ammonium has a Pauling radius of 1.48 Å and a charge of +1; therefore ions capable of substituting for NH_4^+ needed to have a Pauling radius between 1.26 Å to 1.70 Å, and a +1 charge. Additionally, the pure end-member containing the new ion needed to have a melting point that was obtainable with the stage heater apparatus — ideally less than 200 °C. In general, group I ions closely resemble NH_4^+ in chemical behavior (Cotton and Wilkinson, 1980), and potential candidates for substitution with the NH_4^+ ion included Li^+, Na^+, K^+, Rb^+ and Cs^+. Ag^+ also has a similar Pauling radius and was considered.

After a thorough investigation, K^+ was chosen as an experimental candidate primarily by the process of elimination. The Li^+ and Na^+ ions (Pauling radii, 0.6 Å and 0.95 Å respectively) were too small; the Rb^+ and Cs^+ ions (Pauling radii of 1.48 Å and 1.69 Å respectively) might have been possible, but were not used for pecuniary reasons; Ag^+ had a Pauling radius of 1.26 Å, but silver thiocyanate decomposes when heated minimally above room temperature (Alfa Aesar). K^+, however, had a feasible Pauling radius of 1.33 Å (within the required 1.26 Å to 1.7 Å range), and was available commercially in the form of KSCN. Additionally, potassium thiocyanate had a melting point of 173 °C — higher than ammonium thiocyanate (149 °C) but within the range of the stage heater. The 173 °C melting point meant that the $(K, NH_4)SCN$ solid solution should form intermediate composition crystals with good separation between initial and final melting points. This last characteristic was considered advantageous, as it would allow for a wide temperature range in which the textural evolution of crystals could be studied in a melt-present environment, without having to add additional compounds to the system.

The (K, NH_4)SCN solid solution was the only system tested. Solid solution compositions between KSCN and NH_4SCN are defined in terms of KSCN mole fraction (X_K) where;

$$X_K = \frac{n_{NH_4SCN}}{n_{NH_4SCN} + n_{KSCN}} \quad \text{and} \quad X_{NH_4} = \frac{n_{KSCN}}{n_{NH_4SCN} + n_{KSCN}}$$

n_{NH_4SCN} = number of moles of NH_4SCN
n_{KSCN} = number of moles of KSCN

3.3 Crystallization Experiments

Crystallization experiments were designed and executed in order to achieve two primary goals: (1) determine the melting point intervals characteristic of the synthetic system KSCN – NH_4SCN for the construction of a T - X phase diagram, and (2) investigate the textural characteristics of crystals formed. These experiments were used to form a synthetic system in which textural and chemical features, as well as phase relations, could be predictably reproduced.

Crystallization experiments were designed to overcome two primary obstacles in the system KSCN - NH_4SCN. First, crystals of all compositions within the (K, NH_4)SCN solid solution are hygroscopic (especially crystals with high X_K), and the incorporation of water into the crystal matrix significantly lowers melting points. Second, crystals containing ammonium thiocyanate can sublime when heated according to the equilibrium relation,

$$NH_4SCN\ (s) \leftrightarrow NH_3\ (g) + HSCN\ (g),$$

causing samples of (K, NH_4)SCN to become enriched in X_K.

Phase relations for the KSCN – NH_4SCN system were obtained both in thin section and in sealed capillary tubes. In thin section, phase relations and the textural evolution of solid solution crystals were easy to observe with a polarizing microscope. However, during experimentation in thin section, the deposition of solid material on external surfaces, and visible mass-loss from the samples indicated that the epoxy did not form an impermeable seal at elevated temperatures.

In order to study (K, NH_4)SCN phase relations in a completely sealed system, a separate set of melting point experiments were conducted using sealed capillary tubes. Sealed capillary tubes prevented the escape of volatile components produced by heating of the solid solution, and provided more reliable phase relation data. However, sealed capillary tubes proved unsuitable for the study of textural relations. The data obtained from both types of experiments are therefore presented and discussed in the following chapter.

3.3a Thin section preparation of a two-component system: KSCN – NH_4SCN

Samples of pure ammonium thiocyanate (purity, 97.5% minimum) and pure potassium thiocyanate (purity, 99.0% minimum) supplied by Alpha Aesar were mixed together in varying molar proportions (ex: 3:1, 1:1, 1:3, etc.), and then ground into powders. Small amounts of powder were placed on round microprobe slides, which in turn were placed on a ceramic hotplate. The samples were heated until completely melted (~180 °C), at which point the slides were tapped several times in order to decrease air content and unify the sample melt. At the same time, round cover slips were heated directly on the hotplate; when the sample melted, a cover slip was immediately placed over the sample and pressed into place. Despite the heating of the cover slips, they were usually cooler than the sample and caused the samples to quench — forming an irregularly shaped crystal mush. These samples were then allowed to re-melt (~180 °C), and the cover slips were further pressed with a metal rod. Once the samples were thinned and had a reasonably regular consistency, they were removed from the hotplate. Upon cooling, the boundary between the top cover slip and the microprobe slide was sealed with thin section epoxy (Figure 18) and then reheated to approximately 80 °C for 20 hours to set the epoxy.

Thin section samples were placed in the stage heater apparatus and heated until both initial and final melting points were observed. The rates of heating varied with each sample; the temperature of the system was increased in small increments of 2 °C to 8 °C, after which thermal equilibration was allowed to take place before the temperature was again increased. The distance of the system from thermal equilibrium was determined by net changes in melt fraction; when melt fraction remained constant, the system was considered at thermal equilibrium.

3.3b Thin section preparation of a four component system: KSCN – NH_4SCN – NH_4Cl – $(NH_4)_2[Co(SCN)_4] \cdot nH_20$

The system was prepared by dissolving 1 g NH_4SCN, 1 g KSCN, and 0.2 g CoCl in deionized water. The resulting solution was heated on a hotplate (approximately 85 °C) until a small amount of solid precipitated and a saturated solution was obtained. At the same time, a glass microprobe slide and round cover slip were also heated on the

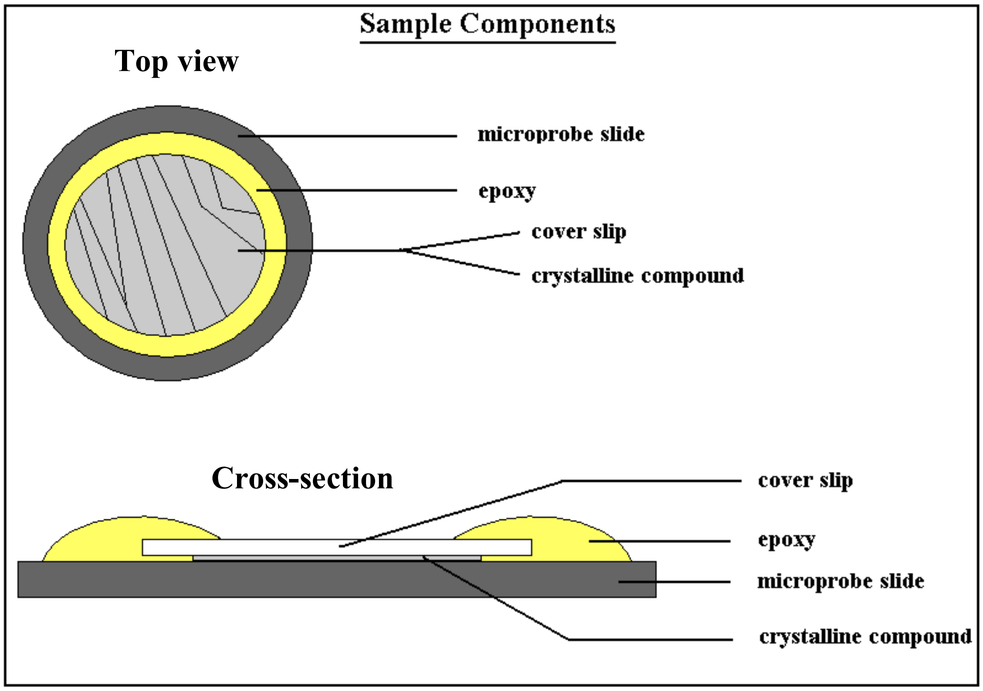

Figure 18: Components of thin sections used for determining (K, NH_4)SCN phase relations.

hotplate. Three drops of the saturated solution were placed on the slide and allowed to lose more water by evaporation. When the sample appeared to be composed of approximately 50% solid and 50% liquid, the hot cover slip was placed on top and pressed into place with a metal rod. The sample was then slowly removed and allowed to cool; after which the sample was sealed with a gel of cyanoacrylates.

The mixing of KSCN (s), NH_4SCN (s), and $CoCl_2$ (s) in deionized water produces a solution from which three solid phases can be precipitated. The solid phases include (1) an isotropic phase containing $(K, NH_4)Cl$, (2) elongate crystals of $[(K, NH_4)_2(CoSCN)_4] \cdot nH_2O$, and (3) blocky crystals of $(K, NH_4)SCN$.

3.3c Sample Preparation: Sealed Capillary Tube Experiments

Solid solution crystals of composition $X_K = (0.75, 0.5, 0.25, 0)$ were prepared by the following procedure: (1) four capillary tubes (2 mm in diameter) were cut to 1 inch in length, and one end of each was fused with a torch; (2) ammonium thiocyanate and potassium thiocyanate were dissolved in deionized water in the aforementioned molar ratios; (3) the resulting solutions were placed on a hotplate and heated to approximately 90 °C in order to evaporate the water and create crystalline material of the desired molar ratios; (4) solid solution crystals were ground into powders and placed within the capillary tubes; (5) the fused ends of the capillary tubes were placed in ice baths for a period of approximately fifteen minutes in order to chill the crystals and prevent volatilization (during the fusing of the other end of the capillary tubes); (6) upon removal from the ice bath, the sealed ends of the capillary tubes were wrapped in wet tissue (also to prevent volatilization), and the open end of the capillary tubes were exposed to a torch for approximately four or five seconds in order to fuse the ends.

Compounds prepared by the capillary-tube procedure (Figure 19) were placed within the stage heater apparatus, and heated at an average rate of 0.5 °C per minute. A sample of composition $X_K = 1$ was also prepared using this procedure, but the sample required more than 50 hours on a hotplate (at 90 °C) to dry. The sample was therefore too hygroscopic to render a meaningful result.

Additional capillary tube samples of $X_K = 1$ and $X_K = 0$ were prepared in a similar manner to the procedure described above, but without steps 2 and 3. This produced "dry" samples that were only exposed to air for a brief period (during the grinding of the compounds and the sealing of the capillary tubes). Additionally, they were not dissolved in deionized water to create crystals of intermediate composition. In reducing the exposure of the compounds to water, they did not have the opportunity to absorb large quantities of water. The melting point difference between "dry" $X_K = 0$ and "wet" $X_K = 0$, was used to evaluate the effect of the sample preparation procedure (especially steps 2 and 3) in the determination of (K, NH_4)SCN phase relations.

3.4 Error

During the preparation of both thin section samples, as well as capillary samples, the loss of NH_3 (g) and HSCN (g) is a concern. In samples initially containing NH_4SCN and KSCN, the loss of NH_3 could concentrate K within the remaining solid—a factor that would explain final melting points that appear high for the starting composition.

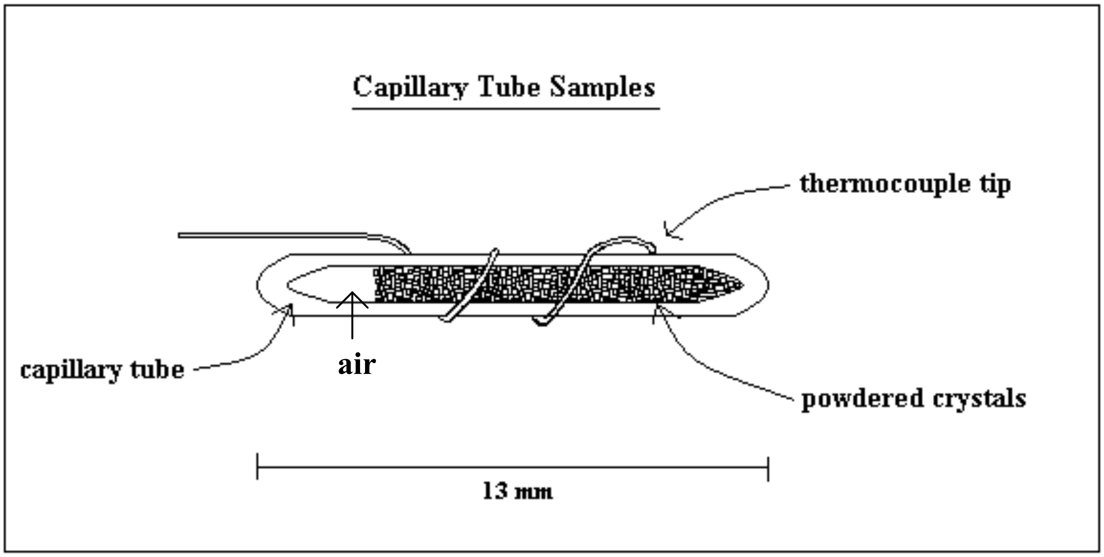

Figure 19. Diagram of a capillary tube sample, including: capillary tube, thermocouple tip, and powdered crystals.

However, both NH_4SCN and KSCN are hygroscopic, and will absorb water directly from the atmosphere. In turn, the addition of water to the system will lower the observed melting points. It is also possible that (in both thin section and capillary samples) temperature gradients within a sample may have affected observed melting points.

The optical determination of a melting point can be difficult; solid-solid phase transitions can appear optically similar to the initiation of melting. Both types of phase transition begin with small changes in interference colors due to volume changes in solids, and the changes occur on a (small) scale that prevents identification until the change has affected at least 3% of the field of view. In each experiment, initial melting points were considered to be the temperature at which visual changes began, and included criteria such as changes in interference colors (due to the thinning of crystals), as well as small changes in grain boundaries. In addition, the temperature of initial melting was confirmed by the observation of flow processes or notable increases in volume of extinct areas (under cross polarized light). These two values for melting points form the error bar limits depicted on both the thin section and capillary tube phase diagrams.

Final melting points were relatively easy to determine, as the microscope field of view was black under cross polarized light. Final melting points were confirmed by dropping the temperature of the sample 1 °C just before melting was complete (~ 98% melt). The initiation of crystallization by the 1 °C drop in temperature was used as evidence that the apparatus was in thermal equilibrium with the sample.

The stage heater apparatus was designed to minimize temperature gradients within samples; thin sections, however, varied in temperature ± 2 °C from the center of the sample to the outer edge, with the coolest area in the center. This was determined by placing the thermocouple tip on the surface of the thin section, and then moving the tip from the center to the outer sample boundary. Capillary tubes contained potentially larger temperature gradients (they could not be positioned precisely horizontal within the apparatus), and the gradient could not be measured due to the wrapping of the thermocouple around the samples. In order to minimize the potential for error due to temperature gradients, all data obtained from capillary tubes pertain to the observation of material not more than 1.5 mm from the thermocouple tip.

During melting point experiments, it was important to heat samples slowly in order to allow thermal equilibration between the circular heater, the thermocouple tip, and the center of the samples. If heat was added to the system too quickly, the temperature controller would appear to “overshoot”, and the measured temperature would elevate much higher than the temperature at which the controller was set. This condition was caused by thermal disequilibrium between the heating element and the thermocouple tip. Additionally, it was also possible to heat the apparatus faster than the center of a sample could equilibrate; thus melting points would appear higher than their true values. Both of these problems were addressed by (1) adding heat at a rate that allowed the thermocouple tip to remain in close thermal equilibrium with the heating element (i.e. 0.5 °C / minute), and (2) adding additional heat to the system in controlled steps; the samples must have visually appeared to have finished equilibration (with the petrographic microscope) before another heating step was initiated.

During both thin section experiments and capillary tube experiments, it was assumed that pressure and volume remained constant for the purpose of constructing X – T phase diagrams. However, due to the equilibrium relationship,

$$NH_4SCN\ (s) \leftrightarrow NH_3\ (g) + HSCN\ (g)$$

at elevated temperatures, the presence of gases within capillary tube samples of constant volume probably caused an increase in pressure. In thin sections, a gas-permeable epoxy was used, allowing both pressure and volume to change. It is not known if changes in pressure or volume had a significant effect on the system.

The stage heater apparatus was calibrated by testing the melting point of a sample of pure indium (purity, 99.999%; Alfa Aesar). Indium wire with a diameter of 0.5 mm was sealed inside a capillary tube, placed within the stage heater apparatus, and heated until melting was observed. The accepted melting point of indium is 156.17 °C (Alfa Aesar), and the experimental melting point obtained with the stage heater apparatus was 157 °C. This result varied less than 1°C from the published melting point of indium, and was also less than the published accuracy of the chromel / alumel thermocouple ($^{+}/\text{-}1$ °C). Thus, no correction has been applied to experimental melting point values obtained with the stage heater apparatus.

Chapter 4

Phase Relation Experiments with the (K, NH_4)SCN Solid Solution

4.1 Phase relations produced from thin section experiments

In order to construct the phase diagram (Figure 20), thin section samples were placed within the petrographic stage heater apparatus and heated until both initial and final melting points were observed. Only one solid phase was observed throughout the temperature ranges of the experiments, and temperature separation between initial and final melting points exists for solid solution crystals with compositions between X_K = 0.75 and X_K = 0.25. A maximum separation of 66 °C between initial and final melting points was obtained for crystals with composition X_K = 0.25. These results are consistent with a binary solid solution model.

The melting point of pure KSCN in thin section was close (within 3.2 °C) to that of the value for KSCN (172.3 °C) provided by the commercial supplier, Alfa Aesar, but the same was not true for pure NH_4SCN. With an observed melting point of 115 °C, the result obtained from thin section was more than 34 °C lower than the expected melting point of NH_4SCN (149.6 °C; Alfa Aesar). This anomalous result is attributed to the hydroscopic nature of NH_4SCN; a small amount of water may have been absorbed by the sample during preparation. However, the melting point of NH_4SCN is still higher than the general trend suggested by the melting points of crystals with intermediate composition, which may actually reflect a dehydration of the system during the experiment. Crystals between X_K = 0.75 and X_K = 0.20 exhibit initial and final melting points that decrease sharply with increasing NH_4SCN content. Samples with composition

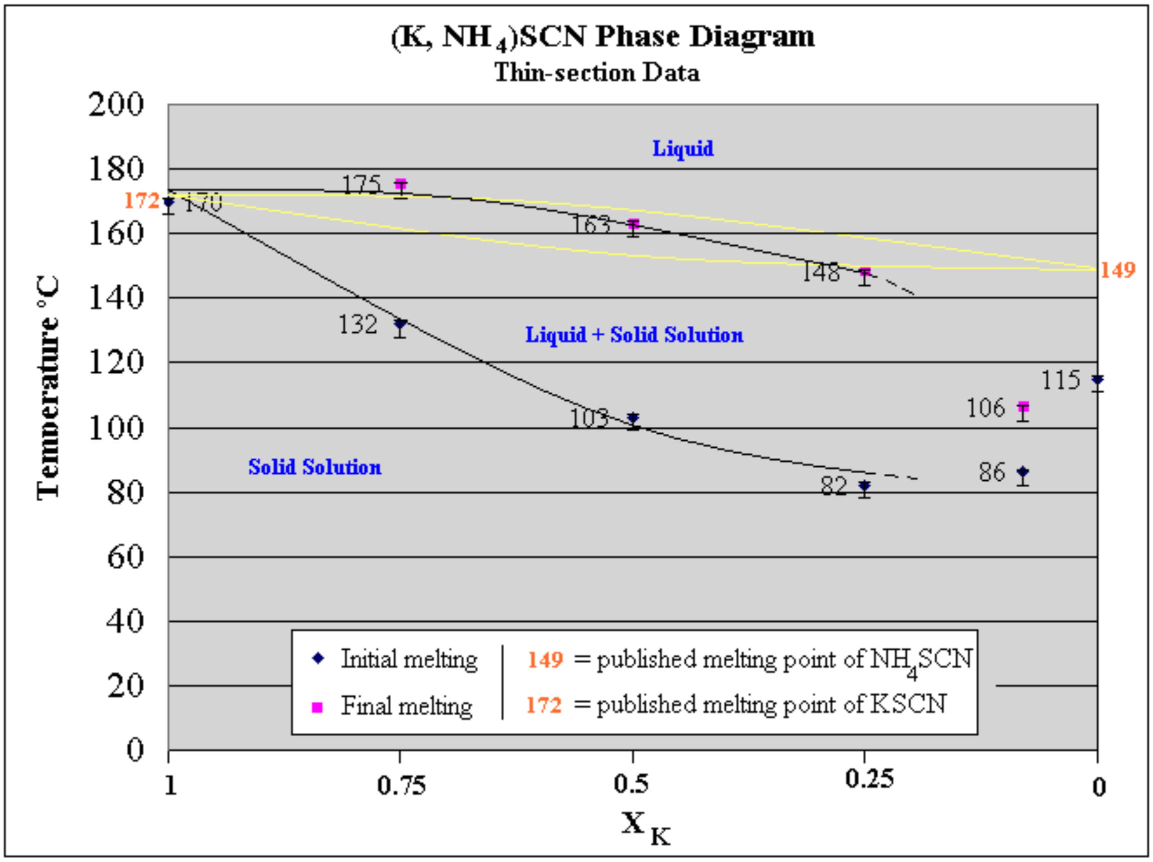

Figure 20: Equilibrium T-X phase diagram for the pseudo-binary system KSCN - NH_4SCN obtained from observations in thin section. Blue diamonds indicate initial melting points (or single melting points for solid solution end-members), and pink squares represent final melting points. The error bars are described in the text. Lines represent hypothetical phase boundaries assuming simple binary solid solution.

$X_K = 0.75$ to $X_K = 0.2$ had initial melting points that were lower than the melting point of pure NH_4SCN (149.6 °C), and samples of composition $X_K = 0.25$ and $X_K = 0.2$ also had final melting points below 149 °C. These low melting points are thought to be due to the absorption of water by the thiocyanate compounds during sample preparatioin. Observed phase relations, however, are consistent with that of a binary solid solution; pure end-members have single melting points, and separation (43 – 66 °C) is obtained between initial and final melting points for samples of intermediate composition ($X_K = 0.75 - X_K = 0.25$).

4.2 Phase relations obtained from capillary tube samples

Sealed capillary tubes provided an environment in which the loss of volatile material was limited. Unlike the thin sections, the capillary tubes were completely sealed preventing NH_3 (g) and H_20 (g) from escaping the system, and the data obtained from these experiments is presented in Figure 21.

Separation between initial and final melting points existed for solid solution crystals of intermediate composition between $X_K = 0.75$ and $X_K = 0.25$. In general, the system provided phase relations consistent with a binary solid solution. The melting point of pure KSCN in a capillary tube was close (within 5.2 °C) to that measured in thin section, but the melting point of pure NH_4SCN was considerably lower than the expected value (based upon data supplied by Alfa Aesar). With an observed melting point of 91 °C, the result obtained from a capillary tube sample was more than 58 °C lower than the

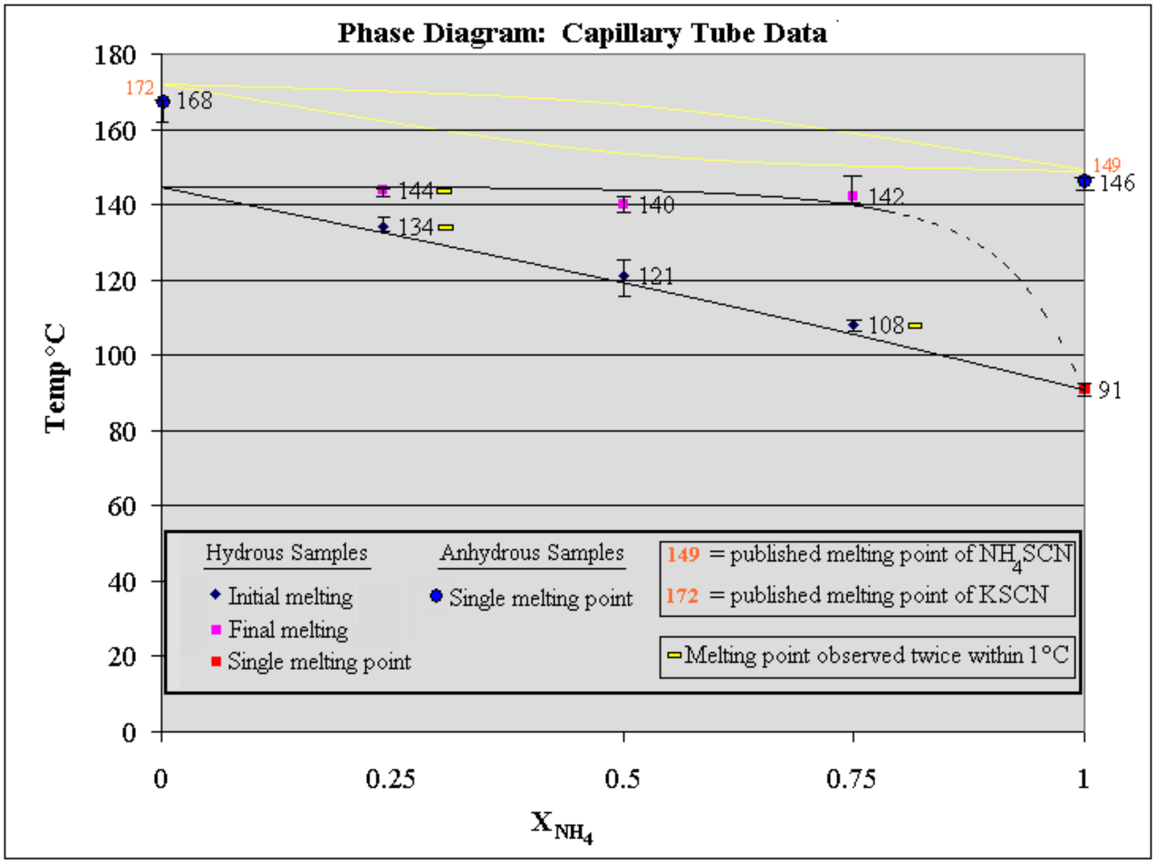

Figure 21: T-X phase diagram of the (K, NH_4)SCN solid solution constructed from capillary tube data. The blue diamonds represent initial melting points, and the pink squares represent final melting points. The red square represents the melting point of a sample with $X_{NH_4} = 1$, prepared by dissolution in deionized water. Blue circle represent the melting points of compounds with composition, $X_{NH_4} = 0$ and $X_{NH_4} = 1$, that were not dissolved in water during preparation. Yellow bars indicate melting points that were observed more than once. The error bars were determined observationally.

expected melting point of NH_4SCN. Again, this anomalous result is attributed to the hydroscopic nature of NH_4SCN; if NH_4SCN incorporated water into its crystal matrix, the melting point of the compound would be significantly reduced. In order to test this conclusion, the melting point of an anhydrous sample (not dissolved in deionized water during preparation) of NH_4SCN was tested; a melting point of 146 °C was obtained. Pure, anhydrous KSCN was also tested, and a melting point of 168 °C was obtained. The samples that were not dissolved in deionized water had melting points relatively close to their accepted values. Samples that were prepared by dissolution in deionized water (before crystallization), however, gave melting point values that were probably affected by the presence of water within the crystal matrix. Future studies involving the (K, NH_4)SCN binary solid solution might obtain more predictable melting points if water content is strictly controlled.

Chapter 5

Textural Experiments with the (K, NH_4)SCN Solid Solution

Textural experiments were conducted in order to investigate: (1) the conditions needed to produce optically visible chemical zoning, and (2) the occurrence of grain boundary migration. All textural experiments were conducted with thin section samples. The textural evolution of two systems were studied: (1) the two component system KSCN – NH_4SCN; and (2) the four component system including KSCN - NH_4SCN – NH_4Cl – $(NH_4)_2[Co(SCN)_4] \cdot nH_20$ (derived from the system created by Means and Park, 1994).

5.1 System: KSCN – NH_4SCN

Chemical zoning can often be identified with a polarizing microscope; when an unstrained crystal cannot go completely extinct at any single stage position, chemical variations within the crystal structure may be the cause. Optical effects consistent with chemical zoning, including variable intragranular extinction positions, were observed in samples of composition $X_K = 0.75$ and $X_K = 0.8$ (Figure 22A and 22B) immediately after preparation. Some of the observed extinction patterns are consistent with zoning (Figure 13C).

While the extinction patterns shown in Figure 22A are similar to those produced by chemical zoning, it is possible that they were produced by strain during the intergrowth of the crystals. However, no external stresses were applied to the sample during preparation.

Samples that appeared to contain zoned crystals were not exposed to heat (other than that required of the preparation process); samples of (K, NH_4)SCN that were heated and cooled in the stage heater apparatus did not produce apparent zoning patterns. The lack of zoning patterns in heated crystals of (K, NH_4)SCN can be attributed to two possible reasons. First, the escape of NH_3 (g) and HSCN (g) at temperatures over 150 °C could not be entirely prevented, thus allowing a loss of NH_4SCN. With complete loss of NH_4SCN, the remaining sample would retain only KSCN, and chemical zoning would not be possible. In an effort to prevent the loss of material, the thin sections were sealed with thin section epoxy; other sealants including cyanoacrylates, and silicate cement (sodium silicate) were tested as thin section sealants, but thin section epoxy allowed the least amount of material to precipitate on external surfaces (during heating). Second, samples may not have been cooled quickly enough to produce chemical zoning; crystals that produced patterns resembling chemical zoning were quenched in air. Samples heated to the liquidus within the stage heater apparatus, and then cooled, may have had time to chemically equilibrate during cooling, thus preventing chemical zoning. Future textural studies using the (K, NH_4)SCN solid solution may require the means to rapidly cool the synthetic crystal mush within the stage heater apparatus, as well as prevent the loss of NH_3 (g) and HSCN (g) at temperatures over 150 °C.

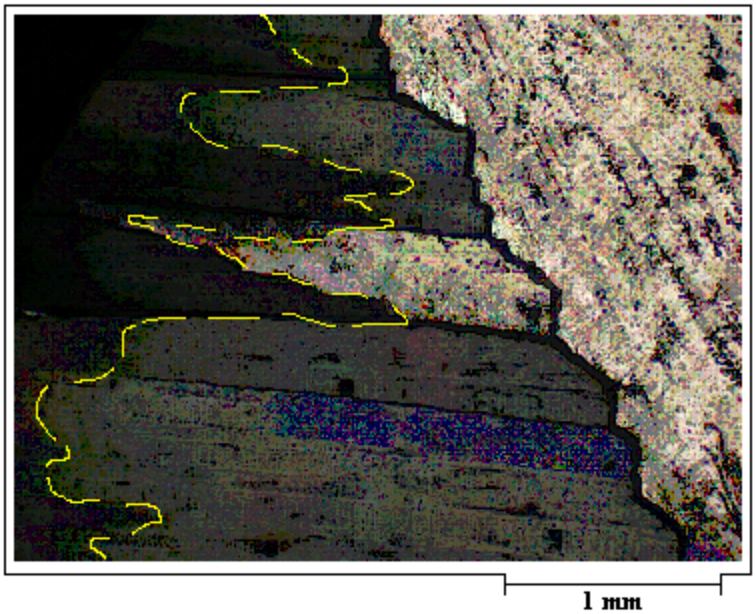

Figure 22A. Photomicrograph of solid solution crystals with composition $X_K = 0.75$ under cross polarized light. Apparent zoning patterns are marked with dashed yellow lines.

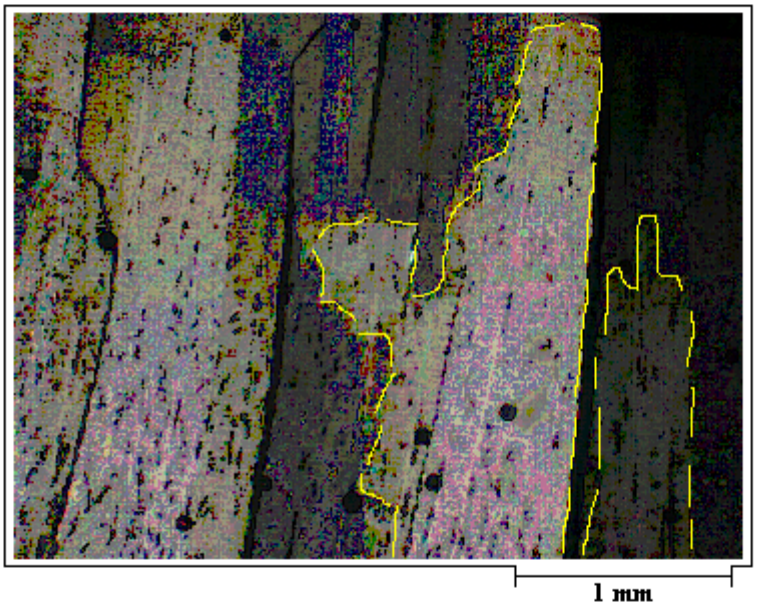

Figure 22B: Photomicrograph of solid solution crystals of composition $X_K = 0.75$ under cross polarized light. Apparent zoning patterns are marked with dashed yellow lines.

5.2 Four component system: KSCN - NH_4SCN – NH_4Cl – $(NH_4)_2[Co(SCN)_4] \cdot nH_20$

The addition of cobalt compounds (i.e. $CoCl_2$) and water to the (K, NH_4)SCN system created an environment in which (K, NH_4)SCN solid solution crystals could form within a wide temperature range (approximately 30 to 80 °C) and in the presence of a large volume of melt. The temperatures at which crystallization took place were lower than those needed for crystals in the (K, NH_4)SCN system, thus reducing the loss of NH_3 (g) and HSCN (g). The resulting system produced grains similar to the "white phase" (NH_4SCN), "cube phase" (NH_4Cl), and "blue phase" $(NH_4)_2[Co(SCN)_4] \cdot nH_20$ created by Means and Park (1994), but the "white phase" in the new system consisted of (K, NH_4)SCN solid solution crystals instead of NH_4SCN.

5.3 Results

Thin sections created with the four-component system produced solid solution crystals and melt that illustrate grain boundary migration. Figure 23 contains three photomicrographs (A, B, C) taken in succession during the cooling of the four-component system (ΔT ~ 50 °C) from a temperature of ~80 °C. The growth of three distinct grains, labeled 1, 2, and 3, are shown. Grains 1 and 3 are oriented with c-axes approximately in the plane of the thin section, and grain 2 appears to be oriented with the c-axis at a high angle from the plane of the thin section (grains are elongated along the c – axis). Crystal faces with the highest growth rates are parallel to the c-axis. Grains 1 and 2 share a grain boundary (as do grains 2 and 3), but grains 1 and 3 are not in contact. In Figure 23B, grains 1, 2, and 3 are clearly becoming intergrown, but the grain boundaries still represent the original texture seen in Figure 23A. In Figure 23C, however, the boundary between grains 1 and 2 has a geometry that has changed significantly during cooling (as crystal 2 has grown at the expense of crystal 1). The boundary between crystal 2 and crystal 3 also changes, but less significantly.

Photomicrographs 23A, 23B, and 23C illustrate the development of “white phase” crystal faces, as well as grain boundary migration. In Figure 23A, crystals 1, 2, and 3 are anhedral, while in Figure 23B, crystal 1 begins the development of crystal faces. In Figure 23C, grains 1 and 3 share a single, uninterrupted crystal face. In addition, the final texture produced by the intergrowth of crystals 1, 2, and 3 does not indicate the growth process shown by photomicrographs A, B, and C.

Figure 24 contains another example of the textural evolution of two “white phase” crystals from the same sample described above. Photomicrograph “A” shows two elongated grains, marked 1 and 2, which share a small grain boundary (labeled with an arrow). In photomicrograph B, the boundary between grains 1 and 2 has extended laterally in a predictable manner, and the beginnings of 120° dihedral angles have developed (one of these areas is adjacent to the arrow). In photomicrograph “C”, the only indication that two separate grains existed is a slight difference in interference colors.

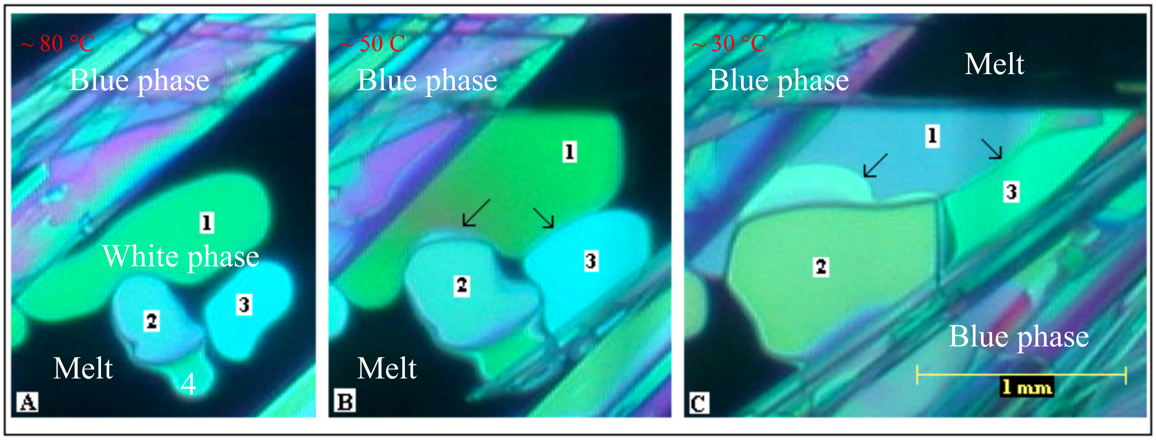

Figure 23. Photomicrograph contains "white phase" solid solution crystals (marked 1, 2, and 3) and "blue phase" crystals. The black areas contain melt, and possibly extinct grains. Changes that took place between photomicrographs A, B, and C illustrate the intergrowth of three crystals and the beginnings of grain boundary migration (marked by arrows).

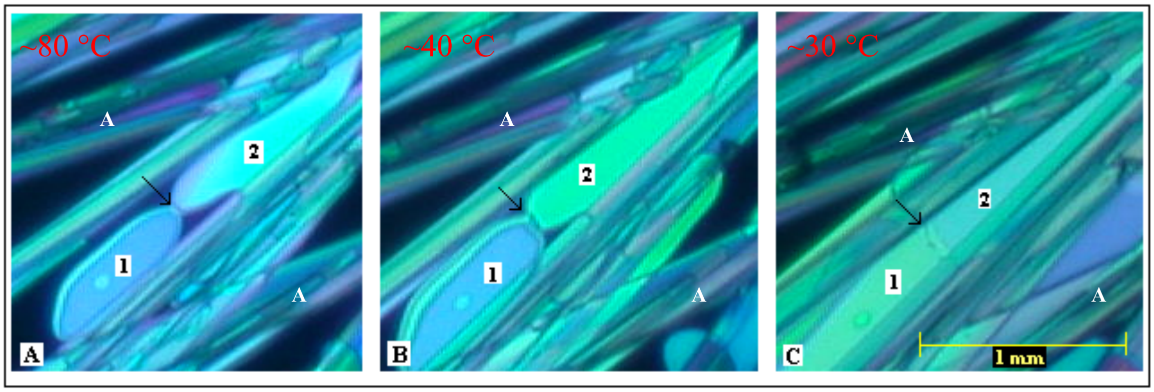

Figure 24: Photomicrograph contains "white phase" solid solution crystals (labeled 1 and 2) and "blue phase" crystals (labeled A) under cross polarized light. The black areas contain liquid (and possibly extinct crystals). Changes that took place between photomicrographs A, B, and C illustrate the intergrowth of two "white phase" crystals; the grain boundary is marked with an arrow.

Conclusion

(1) The petrographic stage heater apparatus was built for the purpose of observing crystallization processes *in situ*, and provided a suitable vessel for experimentation with (K, NH_4)SCN at temperatures below 200 °C.

(2) The use of thin section samples in the petrographic stage heater apparatus allowed the observation of grain boundary development during cooling, including grain boundary migration. Phase relations obtained from samples in thin section, however, appeared to be affected by the sublimation of solid material at temperatures above room temperature. The loss of material could be prevented in future experiments by designing a new type of thin section that does not require epoxy.

(3) The use of sealed capillary tubes during the acquisition of phase relation data was an effective way to prevent the loss of sample material during experimentation with the petrographic stage heater apparatus.

(4) Compounds within the (K, NH_4)SCN system formed a binary solid solution with phase relations comparable to plagioclase, and crystals with extinction patterns consistent with chemical zoning. However, the synthetic compounds were hygroscopic – a factor that affected the phase relations obtained both in thin section and in capillary tubes. While the presence of water in the (K, NH_4)SCN system did not introduce an inappropriate variable for a plagioclase analog (magmatic systems also contain water),

less hygroscopic compounds may be useful in future experiments. While the scope of this study was limited to compounds that were commercially available, others such as RbSCN could be synthesized and potentially used as solid solution end-members.

(5) Thin section samples containing the four component system, KSCN - NH_4SCN - NH_4Cl - $(NH_4)_2[Co(SCN)_4] \cdot nH_20$ were grown at temperatures below 100 °C, and provided the best medium for the study of melt-present grain boundary development.

The (K, NH_4)SCN binary solid solution is an effective plagioclase analog and is capable of producing crystals that may be chemically zoned. Additionally, crystals within the solid solution undergo grain boundary migration. While grain boundary migration has not yet been achieved in zoned crystals, new experiments using different thermal histories (including quenching and annealing) may induce grain boundary migration in zoned crystals. If accomplished, the synthetic binary solid solution could provide valuable microstructural links between processes affecting the development of synthetic textures and the final textures produced during igneous textural evolution.

References

Akers, C., Peterson, S. W., Willett, R. D., A refinement of the crystal structure of KSCN. Acta Crystallographica, B24, 1125 - 1126, 1968.

Alfa Aesar, A Johnson Matthey Company, Supplier of inorganics, organics, metals and materials for research. (800) 343 – 0660, www.alfa.com.

Barnes, S. J., Maier, W. D., Platinum-group elements and microstructures of normal Merensky Reef from Impala platinum mines. Bushveld complex, Journal of Petrology, 43 (1), 103 – 128, 2002.

Bats, J. W., Coppens, P., The experimental charge distribution in sulfur-containing molecules. A study of the deformation density in NH_4SCN at 81 K by combined X-ray and neutron diffraction, Acta Crystallographica, B33, 1542 – 1548, 1977.

Bowen, N. L., The melting phenomena of the plagioclase feldspars. American Journal of Science, 4th series, 34, 577 – 599, 1913.

Cashman, K. V., Textural Constraints on the Kinetics of Crystallization of Igneous Rocks. Reviews in Mineralogy, 24, 259 – 314, 1990.

Chayes, F., Relations between composition and indices of refraction in natural plagioclase. American Journal of Science, Part 1, 85 – 105, 1952.

Cotton, F. A., Wilkinson, G., Advanced Inorganic Chemistry. John Wiley and Sons, New York, 1396 pp., 1980.

Faure, G., Principles and Applications of Geochemistry. Prentice–Hall, Inc., Upper Saddle River, NJ, 1998.

Flood, R. H., Vernon, R. H., Microstructural evidence for the orders of crystallization in granitoid rocks. Lithos, 21, 237 – 245, 1988.

Hibbard, M. J., Petrography to Petrogenesis. Prentice-Hall, Inc., London, 1995.

Hunter, R. H., Textural equilibrium in layered igneous rocks. In I. Parsons (ed.) Origins of Igneous Layering, D. Reidel Publishing Company, 473 – 503, 1987.

Hunter, R. H. Texture Development in Cumulate Rocks. In R. G. Cawthorn (ed.) Layered Intrusions, Elsevier, Amsterdam, 77 – 101, 1996.

Jackson, E. D., Textural Relations of crystal accumulates in the ultramafic zone of the Stillwater complex, Montana. Geological Society of America Bulletin, 65, (12, Part 2), 1268, 1954.

Jackson, E. D., Primary textures and mineral associations in the ultramafic zone of the Stillwater complex, Montana. U.S. Geological Survey Professional Paper, P 0358, 106, 1961.

James, R. S., Hamilton, D. L., Phase Relations in the System NaAlSi3O8 – KalSi3O8-CaAl2Si2O8-SiO2 at 1 Kilobar Water Pressure. Contributions to Mineralogy and Petrology, 21, 111 – 141, 1969.

Kirkpatrick, R. J., Klein, L., Uhlmann, D. R., Hays, J. F., Rates and Processes of Crystal Growth in the System Anorthite-Albite. Journal of Geophysical Research, 84, B7, 3671 – 3676, 1979.

Kirkpatrick, J. R., Theory of nucleation in silicate melts. American Mineralogist, 68, 66 – 77, 1983.

Klement Jr., W., Pistorius, C. W. F. T., Melting and solid-solid transition temperatures at high pressures for NH_4SCN, RbSCN, TlSCN, and CsSCN. Bulletin of the Chemical Society of Japan, 49 (8), 2148 – 2153, 1976.

Kroll, H., Lattice parameters and determinative methods for plagioclase and ternary feldspars. Reviews in Mineralogy, Mineralogical Society of America, 101 – 119, 1983.

Kroll, H., Ribbe, P. H., Lattice parameters, composition, and Al, Si order in alkali feldspars. Reviews in Mineralogy, Mineralogical Society of America, 57 - 98, 1983.

Lofgren, G., An Experimental Study of Plagioclase Crystal Morphology: Isothermal Crystallization. American Journal of Science, 274, 243 – 273, 1974.

Lofgren, G. E., Effect of Heterogeneous Nucleation on Basaltic Textures: A Dynamic Crystallization Study. Journal of Petrology, 24, Part 3, 229 - 255, 1983.

Lowenstein, W., The distribution of aluminum in the tetrahedral of silicates and aluminates. American Mineralogist, 39, 92 – 26, 1954.

MacKenzie, W. S., Donaldson, C. H., Guilford, C., Atlas of igneous rocks and their textures. John Wiley and Sons, Inc., New York, 147 pp., 1991.

Means, W. D., Park, Y., New experimental approach to understanding igneous texture. Geology, 22, 323 – 326, 1994.

McBirney, A. R., Mechanisms of differentiation in the Skaergaard intrusion. Journal of the Geological Society of London, 152, Part 3, 421 – 435, 1995.

Mittlefehldt, D. W., Miller, C. F., Geochemistry of the Sweetwater Wash Pluton, California: Implications for "anomalous" trace element behavior during differentiation of felsic magmas. Geochimica et Cosmochimica Acta, 47, 109 – 124, 1983.

Muncill, G. E., Lasaga, A. C., Crystal-growth kinetics of plagioclase in igneous systems: Isothermal H2O-saturated experiments and extension of a growth model to complex silicate melts. American Mineralogist, 73, 982 – 992, 1988.

Nesse, W. D., Introduction to Optical Mineralogy. Oxford University Press, New York, 301 pp., 1991.

Noble, D. C., Determination of the composition and structural state of plagioclase with the five-axis universal stage. American Mineralogist, 50, 367 – 381, 1965.

Pearce, T., Kolisnik, Al, Observations of plagioclase zoning using interference imaging, Earth-Science Reviews. 29, 9 - 26, 1990.

Ribbe, P. H., Chemistry, Structure and nomenclature of feldspars. Reviews in Mineralogy, Mineralogical Society of America, 1 – 19, 1983.

Smirnov, L. S., Natkaniec, I., Shadrin, Yu. A., Solov'ev, A. I., Neutron diffraction studies of lattice parameters and the phase diagram of $K_{1-x}(NH_4)_xSCN$ solid solution. *Acta* Physica Hungarica, 75, (1-4), 275 – 278,1994.

Smith, J. V., Phase equilibria of plagioclase. Reviews in Mineralogy, Mineralogical Society of America, 223 - 239, 1983.

Tacinelli, J. C., Naslund, H.R., Intercumulus liquid migration in anorthositic blocks of the Skaergaard intrusion. EOS, Transactions, American Geophysical Union, 71 (17), 646, 1990.

Thayer, T. P., Jackson, E. D., A classification of igneous rocks by their history of crystallization and emplacement. U.S. Geological Survey Professional Paper, P 0800-B, B79 – B83, 1972.

Thompson, J. B., Jr., Local equilibrium in metasomatic processes, in Abelson, P. H., ed., Researches in Geochemistry. New York, John Wiley & Sons, 427 – 457.

Tsukamoto, K., In situ observation of mono-molecular growth steps on crystals growing in aqueous solution. Journal of Crystal Growth, 61, 199 – 209, 1983.

Tsukamoto, K., Abe, T., Sunagawa, I., In situ observation of crystals growing in high temperature melts or solutions. Journal of Crystal Growth, 63, 215 – 218, 1983.

Wager, L. R., Brown, G. M., Wadsworth, W. J., Types of Igneous Cumulates. *Journal of* Petrology, 1, Part 1, 73 – 85, 1960.

Wager, L. R., Brown, G. M., Layered Igneous Rocks. W. H. Freeman and Company, San Francisco, 588 pp., 1967.

Yoder, H. S., Tilley, C. E., Origin of Basalt Magmas: An Experimental Study of Natural and Synthetic Rock Systems. Journal of Petrology, 3, Part 3, 342 – 532, 1962.

A.1 Table III

Capillary tube experiments

Exp. #	Sample composition (X_K)	Initial melting point (˚C)	Final melting point (˚C)	Observations
01	1	168	168	Phase transitions over temperature range; 127 - 154 ˚C
02	1	137	163	Sample may not have been at thermal equilibrium
03	0.75	134	144	Phase transitions were not distinguishable
04	0.75	135	143	
05	0.5	117 - 124	139 - 141	Phase transitions were not distinguishable
06	0.25	108	140 - 144	
07	0.25	108	149	Sample not in thermal equilibrium with heater
08	0	146	146	Anhydrous. Possible phase transitions at 90 and 123 ˚C
09	0	91	91	Hydrous.

Experiment 01: ($X_K = 1$) The initial temperature of the sample was 29 °C. At 127 °C, visual changes begin to take place that include a "twinkling" effect, and changes in grain boundaries. They may have represented a phase transition, but the changes were not confined to a small thermal boundary, and continued until the sample reached approximately 154 °C. The final melting point was estimated to be 162 °C, with a margin of error of 3 °C. The rates of heating varied throughout the experiment, as heat was added to the system only after thermal equilibrium appeared to have been reached, and changes (including phase transitions) were complete. The experiment was completed in approximately three hours.

Experiment 02: ($X_K = 1$) Small, visual changes began to take place immediately after the addition of heat. The "twinkling" effect was noted between 67°C and approximately 135 °C. Significant changes in grain boundaries took place between 137 °C and 150 °C. At 163 °C, melting took place. Before melting was complete, the temperature of the system was dropped to 159 °C, and crystallization was initiated. The final melting point of the sample was determined to be 163 °C, but it is suspected that the thermocouple was not in thermal equilibrium with the sample.

Experiment 03: ($X_K = 0.75$) The capillary tube sample did not show significant signs of subsolidus acitivity. Initial melting was estimated to take place at 134 °C, and the final melting point was estimated to be 144 °C. The experiment required approximately three hours.

Experiment 04: ($X_K = 0.75$) The capillary tube sample did not show significant signs of subsolidus acitivity. Initial melting was estimated to take place at 135 °C, and the final melting point was estimated to be 143 °C. The experiment required approximately three hours.

Experiment 05: ($X_K = 0.5$) The capillary tube sample began at 25 °C and was heated approximately 1.7 °C per minute until a temperature of 101 °C was reached. At 117 °C, changes began to take place that may have been caused by a phase transition, but the nature of the change was not clear. The sample was subsequently heated from 101 °C to 141 °C over the next two hours. 141 °C was the estimated final melting point.

Experiment 06: ($X_K = 0.25$) Visual changes are significant by 105 °C, but the initial melting point is estimated to have been 108 °C with a margin of error of 3 °C. A large fraction of the sample was melted by 138 °C, thus the temperature was dropped in order to initiate crystallization. Crystallization began almost immediately. The final melting point of the sample was determined to be between 140 °C and 144 °C. The sample was heated such that the 130 °C to 145 °C interval took approximately 1 hour. Overall, the experiment required approximately three hours.

Experiment 07: ($X_K = 0.25$) The initial melting point was approximately 108 °C. Grain boundary changes (possibly due to a phase transition or volume adjustment) are significant at 134 °C. The final melting point was 149 °C, but the thermocouple may not have been in thermal equilibrium with the sample. The experiment required approximately three hours.

Experiment 08: ($X_K = 0_{anhydrous}$) Visual changes began at 90 °C. The final melting point was approximately 146 °C. The experiment required 2.5 to 3 hours.

Experiment 09: ($XK = 0_{hydrous}$) The sample began at 25 °C and was heated at a rate of approximately 1.2 degrees per minute. The final melting point was 91 °C. The experiment required 1 hour and 16 minutes.

A. 2 Table IV

Thin section experiments

Exp. #	Sample composition (X_K)	Initial melting point (˚C)	Final melting point (˚C)	Observations
10	1	170	170	Twinning patterns at 119 ˚C
11	0.75	132	175	
12	0.5	103	163	
13	0.25	82	148	Possible phase transition at 44 ˚C Twinning patterns develop at 55 ˚C
14	0.2	86	106	
15	0	115	115	Possible phase transition at 50 ˚C

Experiment 10: ($X_K = 1$) The initial temperature of the thin section was 24 °C, and consisted of large crystals of KSCN. At 100 °C, some changes in grain boundaries took place. These effects increased with heat up to 130 °C. The final melting point was determined to be between 166 °C and 170 °C. The heating phase of the experiment required approximately two hours. Once the sample was completely melted, it was then quenched. Crystallization began at 150 °C. The sample was then held at 119 °C for a period of 48 hours. During this period of time, crystals within the sample developed some equant grains with 120° dihedral angles, and "tartan-like" twinning.

Experiment 11: ($X_K = 0.75$) The initial temperature of the thin section was 28 °C. At 119 °C, visual changes in grain boundaries began, but were not indicative of melting. At 132 °C, some melt appeared between the grain boundaries. At 171 °C, the rate of melting was very high and the temperature controller was set to 160 °C to stop growth and initiate crystallization. Crystallization began, and the sample was heated to 171 °C. At 17 °C the entire sample melted. The experiment required approximately 1 hour.

Experiment 12: (X_K = 0. 5) The first significant visual changes take place at 103 °C, and are interpreted to be caused by the beginning of melting. Other changes that may coincide with phase changes or volume changes take place at 116 °C, 132 °C, and 138 °C. The sample reached its final melting point at approximately 163°C. The experiment required less than three hours.

Experiment 13: (X_K = 0.25) Melting initially began at 82 °C. Melting was complete at 148 °C. Some changes were noted at 133 °C. The experiment required less than three hours.

Experiment 14: (X_K = 0.2) Melting initially began at 86 °C. Melting was complete at 106 °C. The experiment required less than three hours.

Experiment 15: (X_K = 0) Visual changes began at 75 °C and may have represented a phase change, but melting did not take place until 115 °C. The experiment required less than three hours.

A.3

Photomicrograph Series I: Experiment 16

$X_K = 0.25$

Rapid cooling from 88 °C to 44 °C; Development of tartan twinning

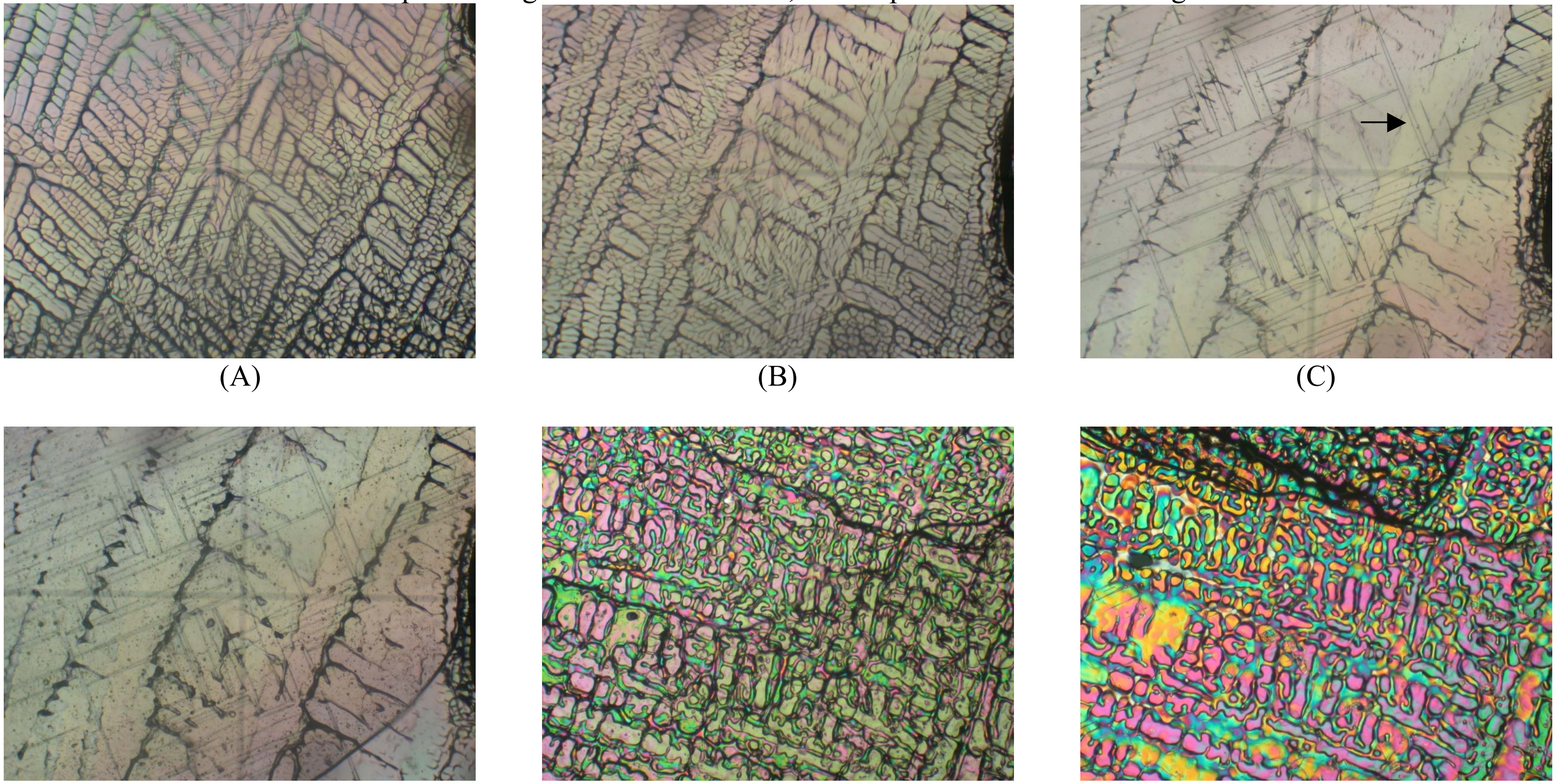

(A)

(B)

(C)

(D)

(A1.) Melting $X_K = 0.25$ (103 °C)

(B1.) Melting $X_K = 0.25$ (103 °C)

Experiment 16
Composition: $X_K = 0.25$
Lighting: Cross polarized light
Thermal trend: Cooling experiment and melting experiment

Remarks:
A melt of composition $X_K = 0.25$ at 147 °C was rapidly cooled by resetting the temperature controller to 0 °C. Crystallization began at > 115 °C. Photomicrographs A through D show a sequence of crystal development between 88 °C and 44 °C in which significant changes in crystal morphology took place (from dendritic to massive, elongated crystals), as well as the development of twinning patterns. The sample was then partially melted at 103 °C (photomicrographs A1 and B1).

Photomicrograph Series II: Experiment 17

Thin-Section Experiment with $X_K = 0.25$, Cross Polarized Light

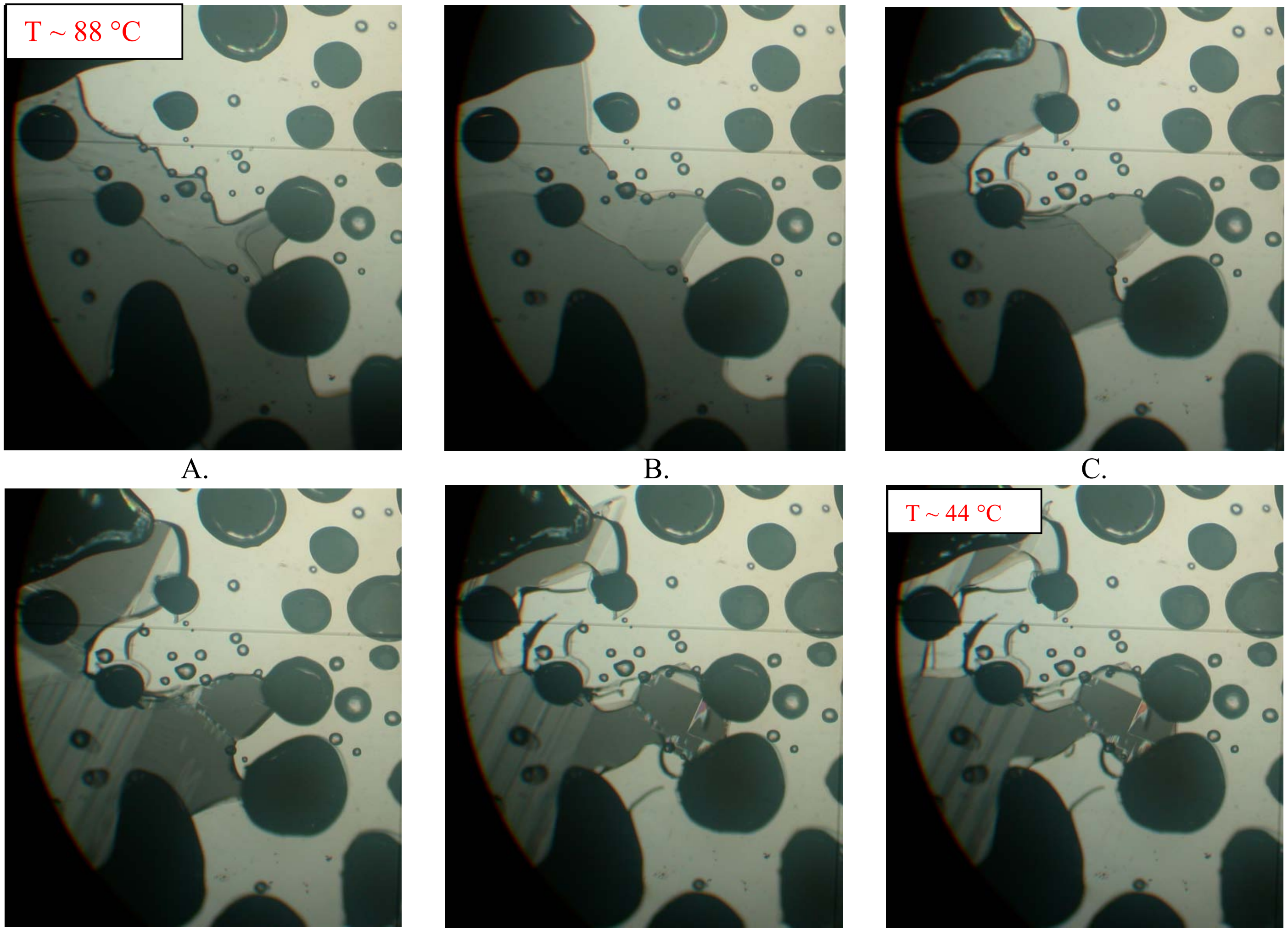

A. B. C.

D. E. F.

Experiment 17

Composition: $X_K = 0.25$
Lighting: Cross polarized light
Thermal trend: Cooling experiment (88 °C – 44 °C)
Time: 15 – 20 minutes

Remarks: The thin section used in this experiment consists primarily of solid crystals of composition $X_K = 0.25$, and gas. Very little (if any) melt is present, but the thin section is riddled with gas bubbles (dark, round spots). However, the boundaries between grains change considerably between photomicrographs A and F while the gas bubbles remain stable. Additionally, crystals in photomicrograph A are untwinned, while the same crystals in photomicrograph F exhibit polysynthetic twins similar to those found in plagioclase crystals. This transformation took place during cooling below the solidus and may mark the transition of the system from orthorhombic to monoclinic.

Photomicrograph Series III: Experiment 18

Zoning patterns, $X_K = 0.75$

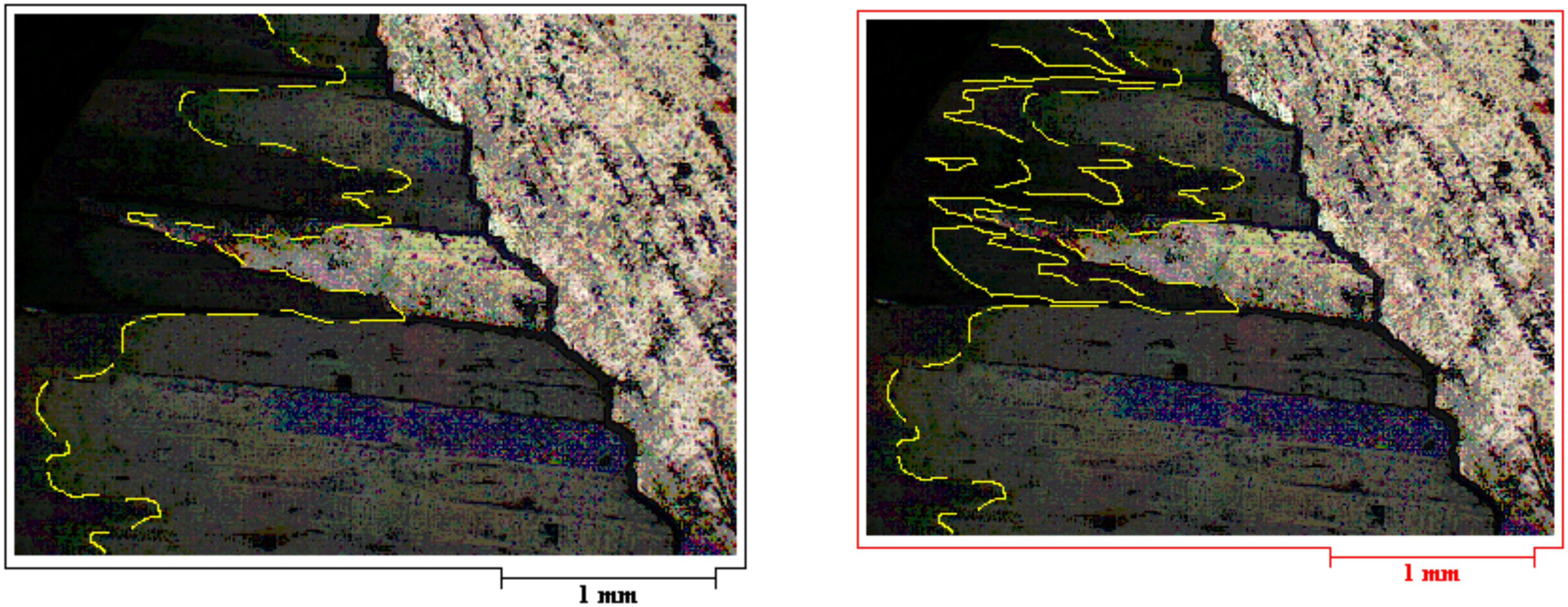

(A) (B)

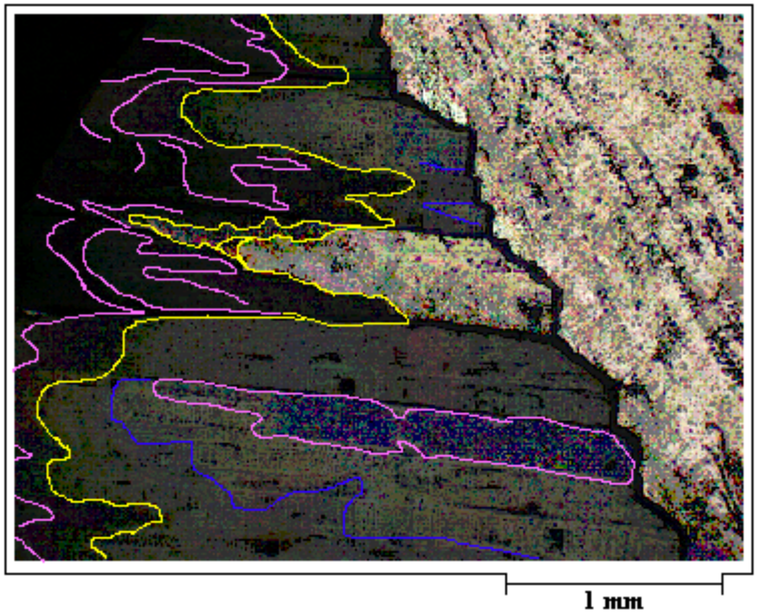

(C)

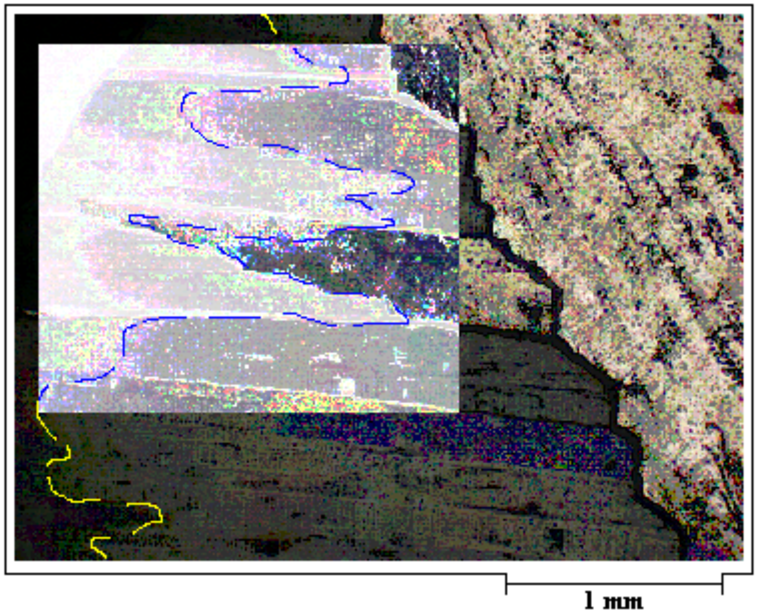

(D)

Experiment 18
Composition: $X_K = 0.75$
Lighting: Cross polarized light
Thermal trend: New sample (quenched product)

Remarks: Photomicrographs A, B, C, and D capture the extinction patterns obtained from a thin section sample with $X_K = 0.75$. The thin section was not heated in the stage heater apparatus. Photomicrograph A is minimally processed, with a single, yellow line outlining one of the most dominant extinction boundaries. Photomicrographs B and C have additional pink and blue lines that outline less distinct boundaries. Photomicrograph D is of the same section, but has had a section of the field of view digitally reversed — a process that seems to make some extinction boundaries more visible.

Photomicrograph Series IV: Experiment 19

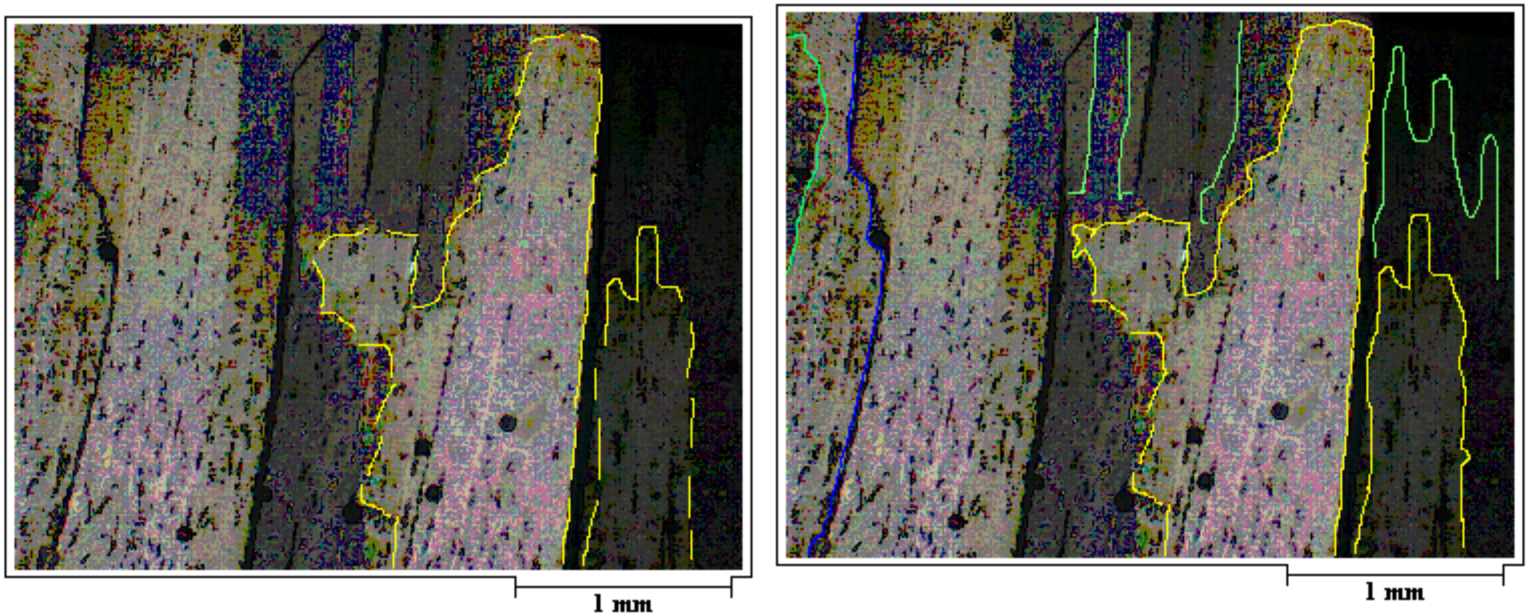

(A) (B)

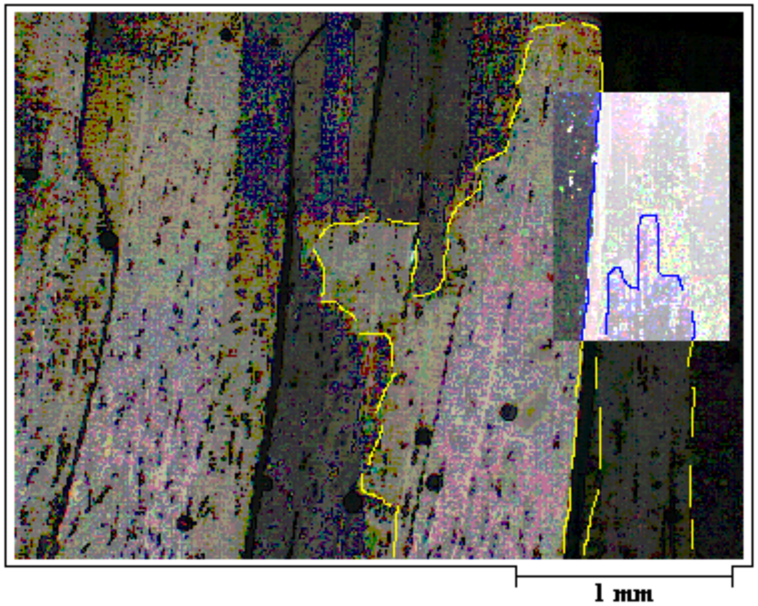

(C)

Experiment 19
Composition: $X_K = 0.75$
Lighting: Cross polarized light
Thermal trend: New sample (quenched product)

Remarks: Photomicrographs A and B show a different area of the same thin section that is shown in Photomicrograph Series VII. The thin section contains crystals of composition $X_K = 0.75$ that have not been subjected to heat in the stage heater apparatus. Yellow lines are used to highlight extinction patterns that may indicate chemical changes within the crystals. One section of the photograph has been processed (with digital color reversal) in such a way that concentric-like zones can be seen.

Photomicrograph Series V

Thin section, $X_K = 0.8$, Stage rotation at room temperature, cross polarized light

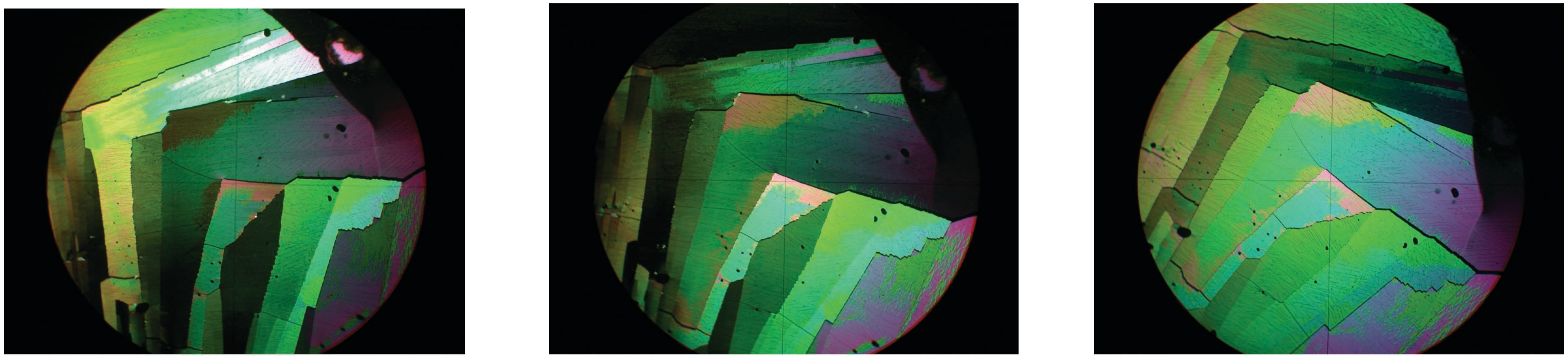

A. B. C.

Photomicrograph Series VI: Experiment 20
Thin section, $X_K = 0.8$, Heating experiment

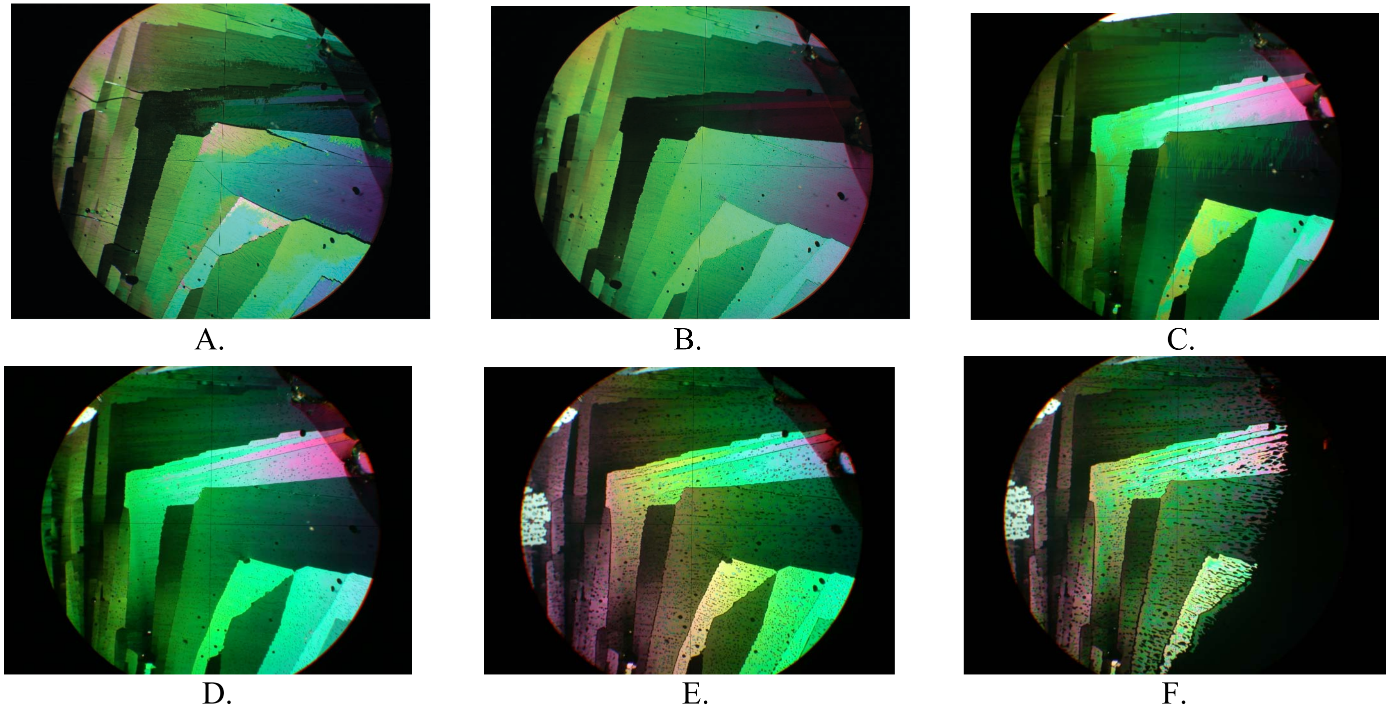

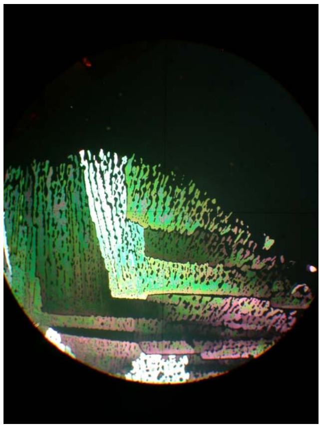

G.

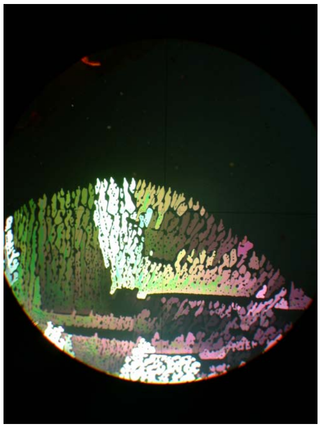

H.

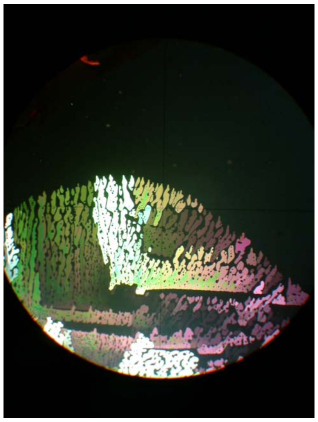

I.

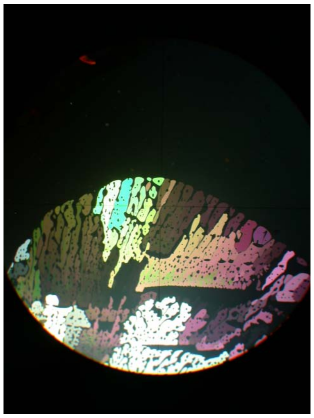

J.

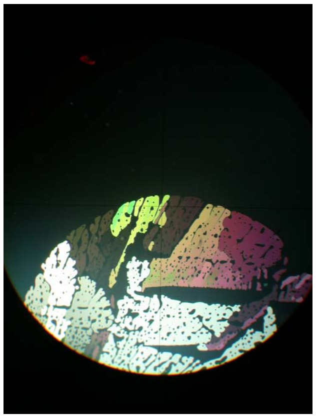

K.

Photomicrograph Series VI
Experiment 20

Composition: $X_K = 0.8$
Lighting: Cross polarized light
Thermal trend: Heating experiment

Remarks:
Heat is added to the system between photomicrographs A through F, and then held stable (± 1 °C) from photomicrographs F through K. Photomicrograph A shows crystals with extinction patterns resembling that of concentric zoning. Upon heating, the crystals quickly appear to homogenize (photomicrograph B). In photomicrograph C, complex extinction patterns develop that may be due to the diffusion of elements from solid to solid, a phase transition, or even the initiation of melting. Ultimately, the cause is not clear.

In photomicrograph E, white crystals begin to appear in the left hand side of the field of view. In photomicrographs F through K, the white crystals grow, but do so by grain boundary migration. The clearly defined melting front suggests that thermal gradients within the apparatus that are large enough to visibly affect melting and crystallization processes.

Photomicrograph Series VII: Experiment 21

Melting Experiment: $X_K = 1$

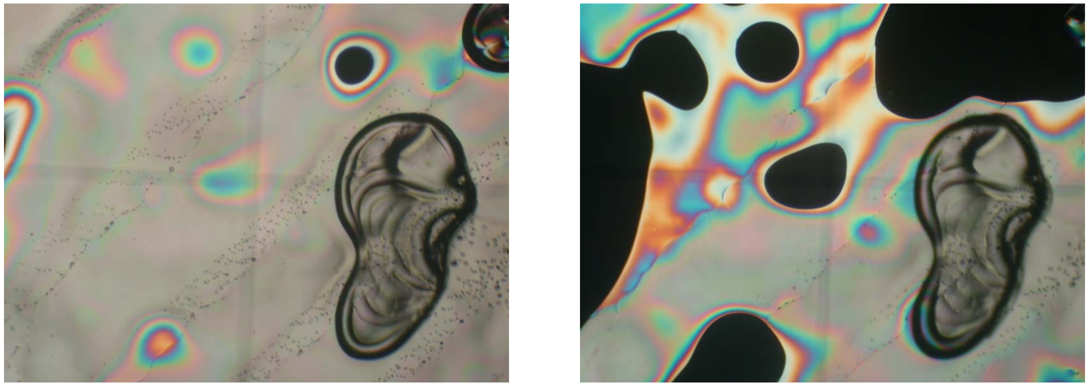

(A)

(B)

Experiment 21
Composition: $X_K = 1$
Lighting: Cross polarized light
Thermal trend: Heating experiment

Remarks:
Photomicrographs A and B were taken when the temperature controller indicated that the sample was 166 °C. The temperature controller was in the process of overshooting its designated temperature, however (it was set on 160 °C), and it continued to heat the sample until it registered at temperature greater than 166 °C). Therefore, the heater, sample, and thermocouple were probably not in thermal equilibrium, and the melting point of 166 °C was inaccurate.

Photomicrographs A and B show the melting of crystals with composition $X_K = 1$. Distinct grain boundaries are not present and the initiation of melting is marked by the appearance of second and third order interference colors at random locations. The areas of color eventually turn black and are composed of melt.

Photomicrograph Series VIII: Experiment 22

Quenching $X_K = 1$ from melt (<150 °C)

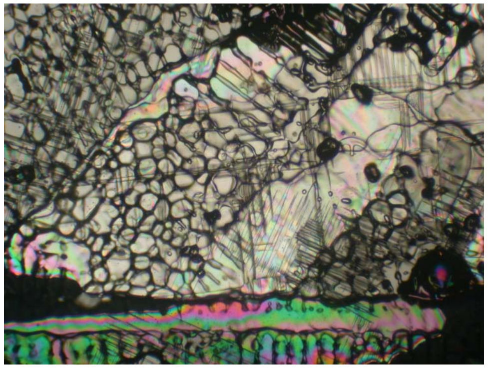

(A)

$X_K = 1$ Annealed overnight (119 °C)

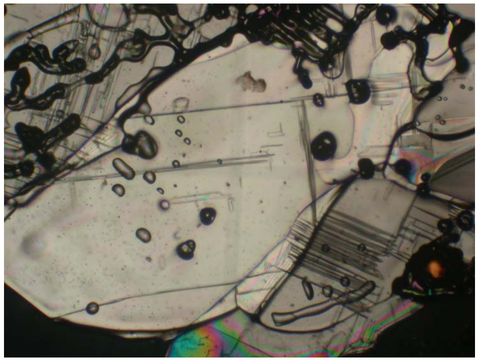

(B)

$X_K = 1$ Annealed overnight (119 °C)

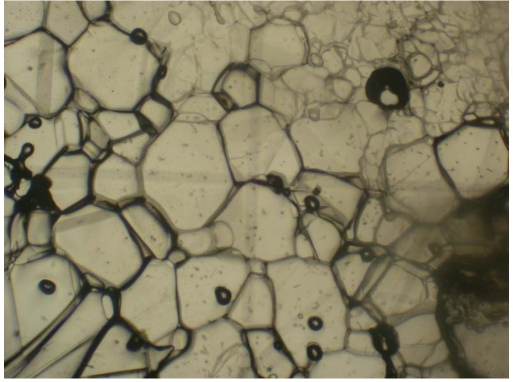

(C)

Experiment 22
Composition: $X_K = 1$
Lighting: Cross polarized light
Thermal trend: Cooling experiment with isothermal stage

Remarks:
A melt of composition $X_K = 1$ at 170 °C was quenched by resetting the target temperature on the temperature controller to 0 °C and allowing the temperature of the system to drop as fast as possible. Crystallization began within 37 minutes at a temperature of approximately 150 °C. Once crystallization was complete, the temperature controller was set to 119 °C and the sample was allowed to anneal for two days. Photomicrographs A, B, and C were taken of the same thin section (different locations) approximately 23 hours after the sample was quenched, and show (1) grain boundaries with 120° dihedral angles (A and C), and grains with twinning patterns similar to feldspar tartan twinning.

(A.4) Stage Heater Assembly

Courtesy of John Arnason